PHYSICS OF FLUIDS **28**, 012002 (2016)

Theoretical description of the gaseous Knudsen layer in Couette flow based on the second-order constitutive and slip-jump models

R. S. Myong[a)]
School of Mechanical and Aerospace Engineering and Research Center for Aircraft Parts Technology, Gyeongsang National University, Jinju, Gyeongnam 52828, South Korea

(Received 15 May 2015; accepted 7 December 2015; published online 7 January 2016)

The Knudsen layer, found in the region of gas flow very close (in order of a few mean free paths) to the solid surfaces, plays a critical role in accurately modeling rarefied and micro-scale gases. In various previous investigations, abnormal behaviors at high Knudsen numbers such as nonlinear velocity profile, velocity gradient singularity, and pronounced thermal effect are identified to exist in the Knudsen layer. However, some behaviors, in particular, the velocity gradient singularity near the surface and higher temperature, remain elusive in the continuum framework. In this study, based on the second-order macroscopic constitutive equation recently derived from the kinetic Boltzmann equation via the balanced closure and cumulant expansion [R. S. Myong, "On the high Mach number shock structure singularity caused by overreach of Maxwellian molecules," Phys. Fluids **26**(5), 056102 (2014)], the macroscopic second-order constitutive and slip-jump models that are able to explain qualitatively all the known non-classical and non-isothermal behaviors are proposed. As a result, new analytical solutions to the Knudsen layer in Couette flow, in conjunction with the algebraic nonlinearly coupled second-order constitutive and Maxwell velocity slip and Smoluchowski temperature jump models, are derived. It was shown that the velocity gradient singularity in the Knudsen layer can be explained within the continuum framework, when the nonlinearity of the constitutive model is morphed into the determination of the velocity slip in the nonlinear slip and jump model. Also, the smaller velocity slip and shear stress are shown to be caused by the shear-thinning property of the second-order constitutive model, that is, vanishing effective viscosity at high Knudsen number. © *2016 AIP Publishing LLC.* [http://dx.doi.org/10.1063/1.4938240]

I. INTRODUCTION

The Knudsen layer (also known as the kinetic boundary layer[1]), found in the region of gas flow very close to solid surfaces, plays a critical role in modeling rarefied and micro-scale gas flows. It is related closely to the fundamental physics of gas transport in micro- and nano-system such as flow between a hard disk, vacuum devices, and vehicles operating in high altitude.[2–6] Just like the conventional boundary layer in viscous gas flows, the Knudsen layer can be found in any gas flow involving a solid wall. As such, the accurate description of the Knudsen layer is a critical issue in the study of rarefied and microscale gases.[5,7–9]

A considerable body of studies on the Knudsen layer from both a kinetic approach, such as the direct simulation Monte Carlo (DSMC), and the higher-order continuum approach has been reported in the past.[10–17] Marques and Kremer[10] showed that in the transition regime and for high Mach numbers, the plane Couette flow problem is well described by Grad's 13 moment theory supplemented by *linear* Maxwell velocity slip and Smoluchowski temperature jump boundary

a)myong@gnu.ac.kr

conditions. Smaller shear stress and non-zero tangential heat flux are identified in both Grad's 13 moment theory and the DSMC. Thatcher[13] and Mizzi[17] additionally identified non-zero normal stress and pronounced thermal effects such as larger difference between central temperature and temperature near the wall at high Knudsen numbers from the solutions of extended macroscopic models of Grad's moment families and DSMC results.

However, although the Knudsen layer has been investigated extensively using the kinetic theory in the past, capturing it within the continuum framework, which will provide distinct advantages in terms of computational efficiency for practical applications of technological interests, has remained a daunting task. The exact underlying mechanisms behind non-classical and non-isothermal behaviors at high Knudsen number in the gaseous Knudsen layer (such as nonlinear velocity profile, smaller velocity slip and shear stress, velocity gradient singularity, larger temperature difference, non-zero normal stress, and tangential heat flux) are not understood fully. In particular, the non-intuitive *velocity gradient singularity*[18] that the flow exhibits the power-law dependence in the Knudsen layer was not predicted by existing higher order continuum theories.[19–22] For example, in the work of Lockerby *et al.*,[20,21] it was claimed from an in-depth assessment of capability of predicting the nonlinearity of the velocity profile that the most common higher-order continuum equation sets, such as Grad's 13 moment,[23,24] Eu's generalized hydrodynamics,[25–27] and Burnett[28,29] and super-Burnett[30] equations, cannot capture the Knudsen layer. It was also argued from the poor performance of variants of these equation families, such as Bhatnagar-Gross-Krook (BGK)-Burnett,[31] that the Knudsen layer cannot be modeled accurately by the majority of higher-order continuum theories, raising serious doubts about the usefulness of these macroscopic models for rarefied and microscale gas flows.

In this work, these unsolved problems of the gaseous Knudsen layer near a solid surface in Couette flow are investigated on the basis of the *nonlinearly coupled second-order* constitutive equation and nonlinear gas-surface molecular interaction model. Recently, independent of the previous continuum approach, a new development has been reported on the constitutive equations of gases in a thermal nonequilibrium (rarefied and microscale) state from the viewpoint of the moment method[32–37] applied to the kinetic Boltzmann equation[38] and the so-called *balanced* closure.[39] An important result obtained from these studies is that the number of places for closing the moment equations is two—kinematic and collision terms—and thus, the order of approximations in handling two terms must be the same, for example, second-order for both kinematic and collision terms. Otherwise, in the case of high Mach number shock structure, the kinematic (stress-strain) coupling term of quadratic nature will grow far faster than the strain rate term due to the destructive interplay, resulting in an imbalance with the first-order dissipation term and eventually a blow-up mathematical singularity. Therefore, to go beyond the first-order accuracy, one must abandon the simple linear relation in the collisional term enjoyed by assuming the simple Maxwellian gas molecule,[29] which was once considered a nice-to-have mathematical coincidence.

As a result of the balanced closure, a nonlinear coupled constitutive relation (called NCCR hereafter) expressed in a mathematically implicit "sinh" form, which is an exact consequence of the Boltzmann equation of monatomic gas within the second-order accuracy, was derived[39]

$$\begin{aligned}
&\rho\frac{D(\boldsymbol{\Pi}/\rho)}{Dt} + 2[\boldsymbol{\Pi}\cdot\nabla\mathbf{u}]^{(2)} + 2p[\nabla\mathbf{u}]^{(2)} = -\frac{p}{\eta}\boldsymbol{\Pi}q_{2\mathrm{nd}}(\kappa),\\
&\rho\frac{D(\mathbf{Q}/\rho)}{Dt} + \frac{D\mathbf{u}}{Dt}\cdot\boldsymbol{\Pi} + \mathbf{Q}\cdot\nabla\mathbf{u} + \boldsymbol{\Pi}\cdot C_p\nabla T + pC_p\nabla T = -\frac{pC_p}{k}\mathbf{Q}q_{2\mathrm{nd}}(\kappa),
\end{aligned} \tag{1.1}$$

where the second-order dissipation term, $q_{2\mathrm{nd}}$, and the first cumulant expansion term, κ, are given in terms of the hyperbolic sine form and a Rayleigh dissipation function,[26] respectively,

$$q_{2\mathrm{nd}}(\kappa) = \frac{\sinh\kappa}{\kappa},\ \kappa = \frac{(mk_B)^{1/4}}{\sqrt{2}d}\frac{T^{1/4}}{p}\left(\frac{\boldsymbol{\Pi}:\boldsymbol{\Pi}}{2\eta} + \frac{\mathbf{Q}\cdot\mathbf{Q}}{kT}\right)^{1/2}.$$

In this expression, ρ, p, T, $\mathbf{u}$, and D/Dt denote the density, the pressure, the temperature, the average velocity vector, and the material time derivative, respectively. Higher-order non-conserved variables $\boldsymbol{\Pi}$ and $\mathbf{Q}$ are the shear stress tensor and the heat flux vector, respectively. The η, k represent the linear (Navier) viscosity and the linear (Fourier) thermal conductivity, respectively.

The d, m, k_B denote the diameter of the molecule, the molecular mass, and the Boltzmann constant, respectively. The symbol $[\,]^{(2)}$ stands for a traceless symmetric part of the tensor and C_p represents the heat capacity per unit mass at constant pressure.

The reason behind the hyperbolic sine form in the dissipation (or production) term of second-order constitutive equation (1.1) can be explained by the observation that the net change in the number of gas molecules due to the Boltzmann collision integral is described by gain minus loss, that is, $\exp^{(\text{nonequilibrium})} - \exp^{(-\text{nonequilibrium})}$, so that the leading term of dissipation in the cumulant expansion[40,41] becomes "sinh."[39] Since the essential physics of fluids at a molecular level (movement and interaction) remains the same, the sinh form is also echoed in other fluids such as non-Newtonian polymer fluid[42] and elastohydrodynamic lubricant.[43]

It should be noted in (1.1) that the locality effect associated with the convective derivative of the term D/Dt will automatically vanish in the case of shear flow since the term $(\mathbf{u} \cdot \nabla)$ is zero by definition ($v = w = 0, \partial/\partial x = \partial/\partial z = 0$). Therefore, a knotty problem associated with a need of additional wall boundary conditions for the shear stress and heat flux inherent in traditional partial differential type constitutive equations that have prevented widespread use of higher-order continuum models in problems of technical interests does not arise in the case of steady-state velocity shear dominated flow. When this NCCR model together with the force terms and the Langmuir slip model[44] was applied to the force-driven compressible Poiseuille gas flow,[32] several important results relevant to the present Knudsen layer have been obtained: First, a kinematic stress constraint and the non-Fourier law embodied in the NCCR model were found to be the ultimate sources of non-classical behavior (the central temperature minimum); second, the role of thermal effect such as the average temperature of the bulk gas flow is critical in describing the high non-equilibrium behavior such as the Knudsen minimum. From these findings, it is expected that the same framework may be able to explain the underlying mechanisms behind the non-classical and non-isothermal behaviors in the Knudsen layer.

The goal of obtaining better understanding of non-classical and non-isothermal effects on the gaseous Knudsen layer from the continuum framework is pursued here by developing an analytical solution to the Knudsen layer in Couette flow, in conjunction with new nonlinearly coupled second-order constitutive and Maxwell velocity slip and Smoluchowski temperature jump models. As noted by Lilley and Sader,[18] the Couette flow velocity profile can be transformed into the reference frame of Kramers' problem using a proper coordinate change and thus, the present Couette flow is sufficient to investigate the Knudsen layer flow. Emphasis is placed on how the new theory is able to explain qualitatively all the known non-classical and non-isothermal behaviors of the gaseous Knudsen layer *within the continuum framework*, in particular the velocity gradient singularity near the surface and the higher temperature at the center. The key idea is to combine two nonlinearities and couplings—*nonlinear coupled* constitutive relation for bulk flow and *nonlinear coupled* boundary conditions at the wall—in seamless way and in the same accuracy of second-order, exactly the same as was done in deriving second-order constitutive equation (1.1). This feature is particularly important since it may be critical in the present Couette flow, which is *driven primarily by moving solid walls*. It will then be demonstrated that morphing of nonlinearity of the second-order constitutive model into the determination of the velocity slip in the nonlinear slip and jump model is just enough to explain all the qualitative properties of the Knudsen layer predicted by the kinetic theory. *To the best knowledge of the author, no hydrodynamic theory to combine the second-order algebraic constitutive relation and the second-order velocity slip and temperature jump model for the study of the Knudsen layer has been reported in the literature*.

Finally, even though analytical solutions to the classical Navier-Stokes-Fourier theory of the planar Couette flow based on the conservation laws with the *first-order* constitutive relation are known in the past, there is room for improvement, for example, central temperature information and rigorous analysis of the effects of temperature dependence of viscosity and thermal conductivity. The precise form of the central temperature in the planar Couette flow is not available in the literature. For this reason, a detailed description of the analytical solutions of the Navier-Stokes-Fourier

equations on the basis of the mathematical technique capable of treating the temperature dependence of viscosity and thermal conductivity in a rigorous way is given in Appendices A and B in order to help the reader to see how they are recovered in near-equilibrium limit from the non-classical second-order solutions.

II. THE SECOND-ORDER CONSTITUTIVE AND SLIP/JUMP BOUNDARY MODELS FOR VELOCITY SHEAR GAS FLOW

From the kinetic Boltzmann equation of the distribution of monatomic gas particles $f(\mathbf{v},\mathbf{r},t)$,

$$\left[\frac{\partial}{\partial t}+\mathbf{v}\cdot\nabla\right]f(\mathbf{v},\mathbf{r},t)=C\left[f,f_2\right], \tag{2.1}$$

where the term $C[f,f_2]$ represents the collision integral of the binary interaction among the particles, the following conservation laws can be derived:

$$\rho\frac{D}{Dt}\begin{bmatrix}1/\rho\\ \mathbf{u}\\ E_t\end{bmatrix}+\nabla\cdot\begin{bmatrix}-\mathbf{u}\\ p\mathbf{I}+\mathbf{\Pi}\\ p\mathbf{u}+\mathbf{\Pi}\cdot\mathbf{u}+\mathbf{Q}\end{bmatrix}=\begin{bmatrix}0\\ \mathbf{0}\\ 0\end{bmatrix}. \tag{2.2}$$

It must be emphasized that these physical conservation laws are the exact consequence of kinetic Boltzmann equation (2.1), valid for all degrees of non-equilibrium. Only after some approximations like the first-order Navier and Fourier (or Chapman-Enskog in kinetic theory terms) constitutive relations,

$$\mathbf{\Pi}_0=-2\eta[\nabla\mathbf{u}]^{(2)}\quad\text{and}\quad\mathbf{Q}_0=-k\nabla T, \tag{2.3}$$

are introduced for the stress tensor and the heat flux vector, they become approximate, thereby valid only at near-thermal-equilibrium. Notice also that second-order NCCR model (1.1) reduces to first-order Navier-Stokes-Fourier constitutive model (2.3) near equilibrium,

$$2p[\nabla\mathbf{u}]^{(2)}=-\frac{p}{\eta}\mathbf{\Pi}_0\quad\text{and}\quad pC_p\nabla T=-\frac{pC_p}{k}\mathbf{Q}_0.$$

In the velocity shear dominated gas flow under steady-state condition, second-order NCCR model (1.1) is further simplified into the following component form:

$$\begin{bmatrix}-4\Pi_{xy}\Pi_{xy_0}/(3\eta)+\underline{0}\\ 2\Pi_{xy}\Pi_{xy_0}/(3\eta)+\underline{0}\\ 2\Pi_{xy}\Pi_{xy_0}/(3\eta)+\underline{0}\\ -\Pi_{yy}\Pi_{xy_0}/\eta-\underline{p\Pi_{xy_0}/\eta}\\ -\Pi_{yz}\Pi_{xy_0}/\eta+\underline{0}\\ \underline{0}\end{bmatrix}=-\begin{bmatrix}\Pi_{xx}p/\eta\\ \Pi_{yy}p/\eta\\ \Pi_{zz}p/\eta\\ \Pi_{xy}p/\eta\\ \Pi_{xz}p/\eta\\ \Pi_{yz}p/\eta\end{bmatrix}q(\kappa),$$

$$\begin{bmatrix}-C_pQ_y\Pi_{xy_0}/(\mathrm{Pr}\,k)-\Pi_{xy}C_pQ_{y_0}/k+\underline{0}\\ -\Pi_{yy}C_pQ_{y_0}/k-\underline{pC_pQ_{y_0}/k}\\ -\Pi_{yz}C_pQ_{y_0}/k+\underline{0}\end{bmatrix}=-\begin{bmatrix}Q_xpC_p/k\\ Q_ypC_p/k\\ Q_zpC_p/k\end{bmatrix}q(\kappa), \tag{2.4}$$

where the underlined terms represent the first-order Navier-Stokes-Fourier terms. Note that the solution of this constitutive equation can be interpreted as a relation to determine the unknown high order flux (like the stress $\mathbf{\Pi}$) for a given input (like strain rate or velocity gradient $\mathbf{\Pi}_0$).

On the other hand, another vital issue, boundary condition at the wall, must be dealt with care before any serious investigation; after all, the Couette flow is generated predominantly by collisions between gas molecules and the moving wall. Traditionally, the following *linear* velocity slip and temperature jump models[45,46] were used as boundary conditions for describing gas-surface

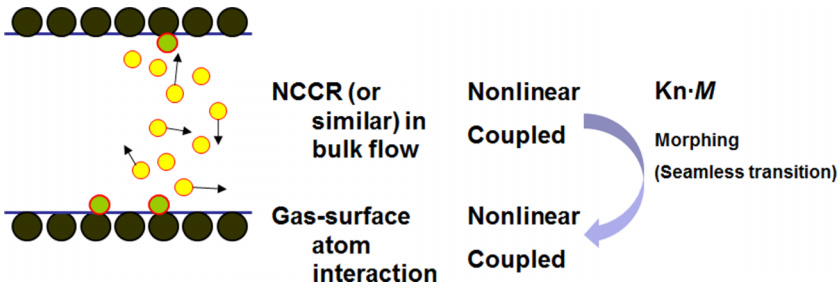

FIG. 1. Combination of two nonlinearities and couplings.

molecular interaction,

$$u(h/2) = V + \sigma_{V_C} l \cdot (-)\left.\frac{\partial u}{\partial y}\right]_{h/2} - \frac{3}{4}\frac{\eta}{\rho T}\left.\frac{\partial T}{\partial x}\right]_{h/2} \text{ and } T(h/2) = T_w + \sigma_{T_C} l \cdot (-)\frac{2\gamma}{\gamma+1}\frac{1}{\Pr}\left.\frac{\partial T}{\partial y}\right]_{h/2}, \tag{2.5}$$

where $l, \sigma_{V_C}, \sigma_{T_C}$ represent the mean free path and the slip and jump constants, respectively. They were obtained after the degree of non-equilibrium is taken as *linear* with the first-order accuracy, from the following original *nonlinear coupled* models in which the velocity slip and temperature jump are determined proportionally by the degree of non-equilibrium near the wall surface,[19,35]

$$u(h/2) = V + \sigma_V l \cdot \left.\frac{\Pi}{\eta}\right]_{h/2} + \sigma_{VT}\frac{3}{4}\frac{(\gamma-1)}{\gamma/\Pr}\left.\frac{Q_x}{p}\right]_{h/2} \text{ and } T(h/2) = T_w + \sigma_T l \cdot \left.\frac{2\gamma}{\gamma+1}\frac{1}{\Pr}\frac{Q_y}{k}\right]_{h/2}, \tag{2.6}$$

where $\sigma_V, \sigma_{VT}, \sigma_T$ represent the slip, thermal creep, and jump coefficients, respectively. But, in this work, a new idea is further introduced such that the coefficients, in particular, the thermal coefficients, are not necessarily constant and are allowed to vary with respect to the degree of non-equilibrium near the surface in the case of second-order approximation, for example, $\sigma_T = \sigma_{T_C}(1 + M \cdot \mathrm{Kn})$. Using these new nonlinear coupled velocity slip and temperature jump models, a seamless combination of two nonlinearities and couplings—NCCR for bulk flow and nonlinear coupled boundary conditions at the wall—can be achieved, as illustrated in Fig. 1, leading to the second-order constitutive and wall boundary models for velocity shear gas flow.

III. SECOND-ORDER ANALYTICAL SOLUTIONS TO THE GASEOUS COUETTE PROBLEM

The plane Couette flow, as illustrated in Fig. 2, is defined as a stationary flow in a slab generated by two identical solid walls oppositely moving with constant speed V. In the gaseous (monatomic) Couette flow problem, the conservation law of mass is automatically satisfied due to the simple relation $v = 0, \partial/\partial x = 0$, imposing no restriction on the density. Then, conservation laws of momentum and energy (2.2) and *second-order* sinh NCCR model (2.4) are reduced to the following system of four differential and nine algebraic equations:[34,39]

$$\frac{d}{dy}\begin{bmatrix}\Pi_{xy}\\ p+\Pi_{yy}\\ \Pi_{yz}\\ \Pi_{xy}u+Q_y\end{bmatrix} = \begin{bmatrix}0\\0\\0\\0\end{bmatrix}, \quad \frac{p}{\eta}\begin{bmatrix}\Pi_{xx}\\ \Pi_{yy}\\ \Pi_{zz}\\ \Pi_{xy}\\ \Pi_{xz}\\ \Pi_{yz}\end{bmatrix} q(\kappa) = \frac{1}{\eta}\begin{bmatrix}(4/3)\,\Pi_{xy}\Pi_{xy_0}\\ -(2/3)\,\Pi_{xy}\Pi_{xy_0}\\ -(2/3)\,\Pi_{xy}\Pi_{xy_0}\\ (p+\Pi_{yy})\,\Pi_{xy_0}\\ \Pi_{yz}\Pi_{xy_0}\\ 0\end{bmatrix},$$

$$\frac{pC_p}{k}\begin{bmatrix}Q_x\\ Q_y\\ Q_z\end{bmatrix} q(\kappa) = \frac{C_p}{k}\begin{bmatrix}\Pi_{xy}Q_{y_0} + Q_y\Pi_{xy_0}/\Pr\\ (p+\Pi_{yy})\,Q_{y_0}\\ \Pi_{yz}Q_{y_0}\end{bmatrix}, \tag{3.1}$$

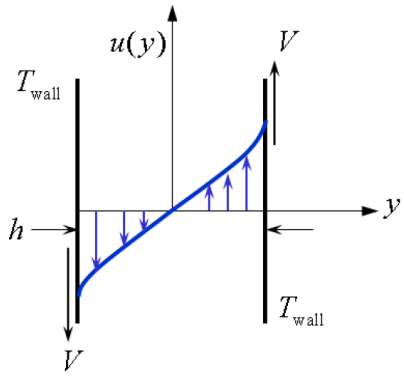

FIG. 2. Description of the pressure-regulated plane Couette gas flow.

where

$$\kappa = \frac{(mk_B)^{1/4}}{\sqrt{2}d}\frac{T^{1/4}}{p}\left(\frac{\Pi_{xx}^2+\Pi_{yy}^2+\Pi_{zz}^2+2\Pi_{xy}^2+2\Pi_{yz}^2+2\Pi_{xz}^2}{2\eta}+\frac{Q_x^2+Q_y^2+Q_z^2}{kT}\right)^{1/2}.$$

From the constitutive relations in (3.1), it can be identified that

$$\Pi_{yz} = \Pi_{xz} = Q_z = 0, \tag{3.2}$$

$$\Pi_{yy} = \Pi_{zz} = -\Pi_{xx}/2. \tag{3.3}$$

In addition, it should be recalled that the thermodynamic driving forces in the system are the velocity and temperature gradients Π_{xy_0}, Q_{y_0}, which are defined in Equation (2.3), that is, the first-order Navier-Stokes-Fourier relations; the dependent variables are $p, \Pi_{yy}, \Pi_{xy}, u, Q_y, T$, and Q_x in the order of appearance in the solutions. When the x, y-momentum equations of the conservation laws in (3.1) is integrated, it can be expressed as

$$\begin{aligned} &\text{constant } \Pi_{xy}(=\Pi_{xy}(0)),\\ &\text{constant } p+\Pi_{yy}(=p(0)+\Pi_{yy}(0)), \end{aligned} \tag{3.4}$$

where 0 on the right-hand side represents the central location $y = 0$.

On the other hand, when the nonlinear function $q(\kappa)$ in the dissipation terms and the driving force Π_{xy_0} are eliminated from the constitutive equations of Π_{xy} and Π_{yy} in (3.1), there is a *kinematic constraint* on the shear and normal stresses, implying their strong inter-dependence,

$$\Pi_{xy}^2 = -\frac{3}{2}\left(p+\Pi_{yy}\right)\Pi_{yy}. \tag{3.5}$$

Other useful relations can be derived from the second-order constitutive relations in (3.1); by combining equations of Π_{xy} and Q_y,

$$\frac{Q_y}{Q_{y_0}} = \frac{\Pi_{xy}}{\Pi_{xy_0}} \tag{3.6}$$

and by combining equations Q_x and Q_y,

$$\frac{Q_x}{Q_y} = \left(1+\frac{1}{\Pr}\right)\frac{\Pi_{xy}}{(p+\Pi_{yy})}. \tag{3.7}$$

In addition, Equations (3.4) and (3.5) together with the x-momentum equation, $d\Pi_{xy}/dy = 0$, yield the following uniform solutions:

$$\Pi_{xy} = \Pi_{xy}(0)(\equiv \Pi),\ p = p(0),\ \Pi_{yy} = \Pi_{yy}(0). \tag{3.8}$$

Furthermore, through relation (3.6), an instructive relation in *cross-stream* distribution of the temperature and stream-wise velocity can be derived. When the energy conservation law is combined with relation (3.6), it is reduced to

$$\frac{d}{dy}\left(Q_y + \Pi_{xy}u\right) = \frac{d}{dy}\left(Q_{y_0}\frac{\Pi_{xy}}{\Pi_{xy_0}} + \Pi_{xy}u\right) = 0. \tag{3.9}$$

After applying $d\Pi_{xy}/dy = d\Pi_{xy_0}/dy = 0$, $u(0) = Q_y(0) = Q_{y_0}(0) = 0$ and definition (2.3), the energy conservation law can be written in an invariant form

$$Q_y + \Pi_{xy}u = Q_{y_0} + \Pi_{xy_0}u = 0 \text{ or } C_pT(y) + \frac{1}{2}\Pr u^2(y) = C_pT(0). \tag{3.10}$$

A close examination reveals that this relation is the same as that of the adiabatic wall (or recovery) temperature $T(0)$ in the laminar boundary layer if the centerline is taken as a wall boundary with no slip. This preservation relation implies that the *cross-stream* variation of stream-wise velocity is directly related to temperature variation and that this property will be pronounced in high speed gas flows. Since the balanced closure with the second-order accuracy is the only major assumption introduced so far, (3.3), (3.5), and (3.7), the constant pressure and stresses and the energy preservation in cross-stream direction (3.10) will hold for any monatomic gases, irrespective of the degree of non-equilibrium and boundary conditions at the solid wall.

Furthermore, when second-order constitutive equation (3.1) and relations (3.6) and (3.7) are combined, the following *implicit* constitutive relations in terms of driving forces Π_{xy_0}, Q_{y_0} can be derived

$$\begin{aligned}
\Pi^*_{xy} &= \frac{3q(\kappa)}{3q^2(\kappa) + 2\left(N_\delta\Pi^*_{xy_0}\right)^2}\Pi^*_{xy_0},\ \Pi^*_{yy} = -\frac{2N_\delta\Pi^*_{xy_0}}{3q^2(\kappa) + 2\left(N_\delta\Pi^*_{xy_0}\right)^2}\Pi^*_{xy_0},\\
Q^*_y &= \frac{3q(\kappa)}{3q^2(\kappa) + 2\left(N_\delta\Pi^*_{xy_0}\right)^2}Q^*_{y_0},\ Q^*_x = \left(1 + \frac{1}{\Pr}\right)\frac{3N_\delta\Pi^*_{xy_0}}{3q^2(\kappa) + 2\left(N_\delta\Pi^*_{xy_0}\right)^2}Q^*_{y_0},
\end{aligned} \tag{3.11}$$

where from definition (1.1), the cumulant κ can be expressed in dimensionless form

$$\kappa = cN_\delta\left[\mathbf{\Pi}^* : \mathbf{\Pi}^* + \frac{2}{(\gamma-1)\Pr M^2}\frac{(\Delta T)^2}{T_rT_w}\frac{1}{T^*}\mathbf{Q}^*\cdot\mathbf{Q}^*\right]^{1/2},\ c^2 = \frac{2\sqrt{\pi}}{5}A_2(\nu)\Gamma\left[4 - \frac{2}{\nu-1}\right].$$

The tabulated values of $c(\nu), A_2(\nu)$ for the exponent of the inverse power law ν are available in the literature,[29,32] for example, $c = 1.0138$ for a Maxwellian molecule. Other normal stresses Π_{xx}, Π_{zz} can be determined by relation (3.3). Note that the first equation in (3.11) shows the shear-thinning property, that is, vanishing effective viscosity at high Knudsen number.[39,44]

In deriving Equation (3.11), the following dimensionless method that is able to treat the temperature dependence of viscosity and thermal conductivity in a rigorous way was employed after several modifications to the initial introduction in the study of the force-driven Poiseuille gas flow,[34]

$$\begin{aligned}
&u^* = u/V,\ \rho^* = \rho/(p/RT_w),\ T^* = T/T_r,\ \Pi^* = \Pi/\left(\eta_wV/h\right),\ Q^* = Q/\left(k_w\Delta T/h\right),\\
&y^* = y/h,\ M = \frac{V}{\sqrt{\gamma RT_w}},\ \mathrm{Kn} = \sqrt{\frac{\pi}{2}}\frac{\eta_w\sqrt{RT_w}}{ph},\ N_\delta = \frac{\eta_wV/h}{p},\ \mathrm{Ec} = \frac{(\gamma-1)M^2}{\Delta T/T_w},\ \Pr = \frac{C_p\eta_w}{k_w},
\end{aligned} \tag{3.12}$$

where the subscripts r, w denote the reference state and the state at the wall, respectively. Here, ΔT denotes $|T(0) - T_w|$. M, N_δ, Kn, and Ec are dimensionless hydrodynamic numbers: Mach number, a composite number, Knudsen number, and Eckert number, respectively. The composite number N_δ is related to other numbers such that $N_\delta = \sqrt{2\gamma/\pi}\,M\,\mathrm{Kn}$.

It must be emphasized that the definition of dimensionless variables and parameters is not unique in general and the present set of definitions is selected after carefully taking into consideration the well-posedness (existence, uniqueness, and continuous dependence on the data) of the present Couette boundary value problem. For example, it will be more effective to choose the wall velocity—which is an input—as the dimensionless velocity in the present wall-driven Couette flow.

On the other hand, the average velocity will be more suitable as the dimensionless velocity in the force-driven Poiseuille flow,[34] since the velocity is not known priori and is the part of the solutions. Furthermore, with the average quantity T_r defined as

$$T_r^n = \frac{h/2}{\int_0^{h/2} T^{-n} dy} \tag{3.13}$$

and with the introduction of a new variable s defined by

$$T^n ds = dy \text{ or } T^{*n} ds^* = dy^* \tag{3.14}$$

in dimensionless form, where $s^* = sT_r^n/h$, the following auxiliary relations hold:

$$s^*\left(y^* = \frac{1}{2}\right) = \frac{1}{2}, \int_0^{1/2} T^{*n} ds^* = \frac{1}{2}. \tag{3.15}$$

Here, n represents a constant defined as $n = 1/2 + 2/(\nu - 1)$, where ν is the exponent of the inverse power laws of gas molecules. For a Maxwellian molecule, $n = 1$, whereas $n = 1/2$ for a hard sphere molecule. It should be emphasized that the second equation in auxiliary relations (3.15) enables the unknown average temperature T_w^* to be determined in terms of M, Kn, the slip and jump coefficients, and the velocity slope.

Then, the system of ordinary differential equations with dependent variables u and T may first be solved in terms of the variable s; the solutions are later expressed in the function of the distance y. The velocity profile in coordinate s^* can be derived from the x-momentum equation or (B2),

$$u^*(s^*) = \Delta s^* \text{ from } \frac{du^*}{dy^*} = \frac{\Delta}{T^{*n}}, \tag{3.16}$$

where

$$\Delta\left(\equiv \frac{du^*}{ds^*}\right) = -\Pi_0^* T_w^{*n}.$$

Now the *velocity slope* Δ will be determined by combining the second-order NCCR constitutive and slip models, (3.11) and (2.6), respectively, repeated below,

$$u^*(s^* = 1/2) = 1 + \sigma_V \mathrm{Kn}\,\Pi^*]_{s^*=1/2} + \sigma_{VT}\frac{3}{4}\frac{(\gamma-1)}{\gamma/\mathrm{Pr}}\frac{k_w \Delta T/h}{pV} Q_x^*]_{s^*=1/2}. \tag{3.17}$$

Note that a creeping term on the right-hand side appears since the tangential heat flux Q_x is generated by the driving force Q_{y_0}, in the case of the second-order NCCR model through relation (3.7). On the other hand, after introducing thermal conductivity $k(T) = k_w(T/T_w)^n$ and using Equation (3.16), the energy equation in conservation laws is reduced to

$$\frac{dQ_y^*}{ds^*} = \mathrm{Pr}\,\mathrm{Ec} T_w^{*n} \Pi_0^* \Pi^*. \tag{3.18}$$

When this is integrated once with respect to s^*, the heat flux in the y-direction can be written as

$$Q_y^* = \mathrm{Pr}\,\mathrm{Ec}\Pi^*(-\Delta)s^* \text{ or } \frac{Q_y}{pV} = N_\delta \Pi^*(-\Delta)s^*. \tag{3.19}$$

Here, the local thermal equilibrium condition at the centerline has been applied: $Q_y^*(0) = 0$. The tangential heat flux is now determined from (3.7),

$$\frac{Q_x}{pV} = \left(1 + \frac{1}{\mathrm{Pr}}\right)\frac{N_\delta^2}{q(\kappa)}\Pi^*\Pi_0^*(-\Delta)s^*. \tag{3.20}$$

Then, when Equations (3.11), velocity profile (3.16), and heat flux (3.20) are applied to (3.17), an algebraic equation of unknown Δ can be derived

$$\frac{1}{2}\Delta = 1 + \Pi_{1/2}^*\left[\sigma_V \mathrm{Kn} + N_\delta^2 \sigma_{VT}\frac{3(\gamma-1)}{8\gamma}(1+\mathrm{Pr})\frac{\Delta^2}{q(\kappa_{1/2})T_w^{*n}}\right]. \tag{3.21}$$

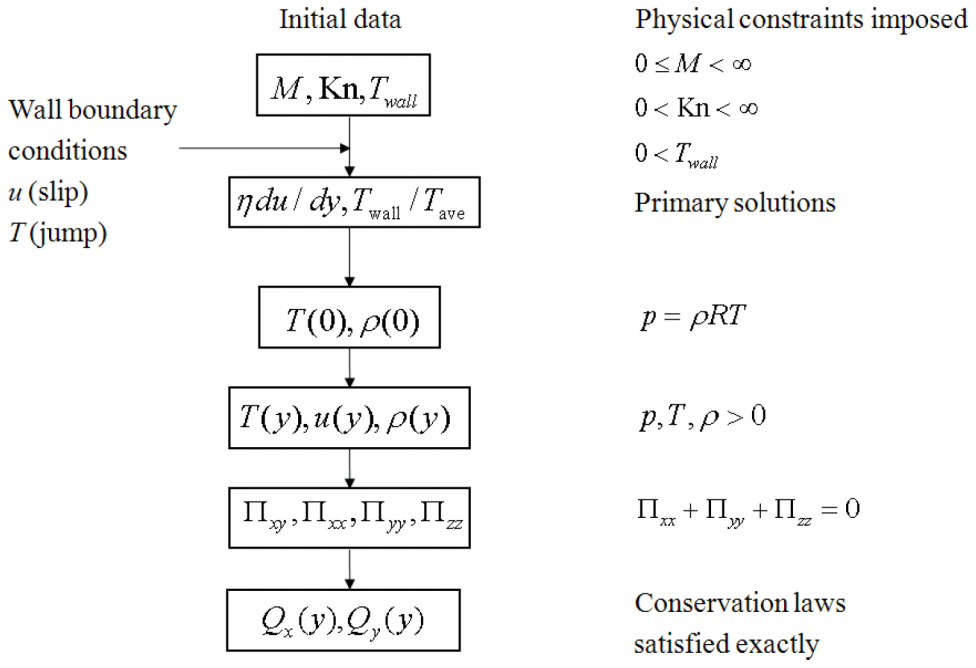

FIG. 3. Construction of unique flow solution for the Couette gas flow.

When the first equation in (3.11) is applied to the term $\Pi^*_{1/2}$, it is reduced to a cubic equation

$$A\Delta^3 - 2\Delta^2 + 3\left(\frac{T_w^{*n}}{N_\delta/q(\kappa_{1/2})}\right)^2\left(\frac{\Delta}{2\alpha_V} - 1\right) = 0, \tag{3.22}$$

where

$$\alpha_V \equiv \frac{1}{1 + 2\sigma_V \mathrm{Kn} T_w^{*-n}/q(\kappa_{1/2})}, \tag{3.23}$$
$$A \equiv 1 + \sigma_{VT}\frac{9(\gamma-1)}{8\gamma}(1 + \mathrm{Pr}),$$

and its analytic solution can be expressed as[47]

$$\Delta = \left(r + \sqrt{g^3 + r^2}\right)^{1/3} + \left(r - \sqrt{g^3 + r^2}\right)^{1/3} + \frac{2}{3A},$$

where

$$g = \frac{1}{2\alpha_V A}\left(\frac{T_w^{*n}}{N_\delta/q(\kappa_{1/2})}\right)^2 - \left(\frac{2}{3A}\right)^2, r = \frac{1}{2}\left(\frac{3}{A} - \frac{1}{\alpha_V A^2}\right)\left(\frac{T_w^{*n}}{N_\delta/q(\kappa_{1/2})}\right)^2 + \left(\frac{2}{3A}\right)^3.$$

Note that Δ has a real solution since cubic equation (3.22) always has a non-negative real root when $0 < \alpha_V \leqslant 1$ for any value of $T_w^{*n} q(\kappa_{1/2})/N_\delta$. It is also interesting to note the limiting behaviors from cubic equation (3.22): $\Delta \to 2\alpha_V (= 2)$ as $N_\delta \to 0$ or ∞, since $\lim_{N_\delta \to 0 \text{ or } \infty} T_w^{*n} q(cN_\delta)/N_\delta \to \infty$.

When Equations (3.6) and (3.19) and the definition of $Q^*_{y_0}$ are combined, the following differential equation for the temperature profile can be obtained:

$$\frac{dT^*}{ds^*} = -(\gamma - 1)\,\mathrm{Pr}\, M^2 T_w^* \Delta^2 s^*. \tag{3.24}$$

Then, the temperature profile can be written as

$$T^*(s^*) = T^*(0) - \frac{(\gamma - 1)}{2}\,\mathrm{Pr}\, M^2 T_w^* \Delta^2 s^{*2}. \tag{3.25}$$

TABLE I. Comparison of the first-order Navier-Stokes-Fourier and the second-order NCCR solutions.

Items	NSF with constant coefficients	NSF with varying coefficients	Second-order model with varying coefficients
p	$p(0)$	$p(0)$	$p(0)$
$\frac{du^*}{dy^*}$	$2\alpha_{V_C}$	$\frac{2\alpha_{V_0}}{T^{*^n}}$	$\frac{\Delta}{T^{*^n}}$
u^* $\left(\equiv \frac{u}{V}\right)$	$2\alpha_{V_C} y^*$	$2\alpha_{V_0} s^*$	Δs^*
Δ $\left(\equiv \frac{du^*}{ds^*}\right)$	$\Delta_C = 2\alpha_{V_C}$	$\Delta_0 = 2\alpha_{V_0}$	$A\Delta^3 - 2\Delta^2 + 3\left(\frac{T_w^{*n}}{N_\delta / q(\kappa_{1/2})}\right)^2 \left(\frac{\Delta}{2\alpha_V} - 1\right) = 0,$ $A \equiv 1 + \sigma_{VT} \frac{9(\gamma-1)}{8\gamma}(1+\Pr)$, where $\sigma_{VT} = 1 + cN_\delta/2$
T_w^*	$T_w^* = \left[1 + E_C^2\left(1 - \frac{\alpha_{T_C}}{3}\right)\right]^{-1}$	$T_w^* = \left[1 + E_0^2\left(1 - \frac{\alpha_{T_0}}{3}\right)\right]^{-1}$ for Maxwellian	$T_w^* = \left[1 + E^2\left(1 - \frac{\alpha_T}{3}\right)\right]^{-1}$ for Maxwellian
α_V	$\alpha_{V_C} = \frac{1}{1+2\sigma_{V_C}\mathrm{Kn}}$	$\alpha_{V_0} = \frac{1}{1+2\sigma_{V_C}\mathrm{Kn}T_w^{*-n}}$	$\alpha_V = \frac{1}{1+2\sigma_V \mathrm{Kn} T_w^{*-n}/q(\kappa_{1/2})}$, $\sigma_V = \sigma_{V_C}$
α_T	$\alpha_{T_C} = \frac{1}{1+4\sigma'_{T_C}\mathrm{Kn}}$		
		$\alpha_{T_0} = \frac{1}{1+4\sigma'_{T_C}\mathrm{Kn}T_w^{*-n}}$, where $\sigma'_{T_C} \equiv \frac{2\gamma}{\gamma+1}\frac{1}{\Pr}\sigma_{T_C}$	$\alpha_T = \frac{q(\kappa_{1/2}) + 2(N_\delta \Delta T_w^{*-n})^2/3 q(\kappa_{1/2})}{[q(\kappa_{1/2}) + 2(N_\delta \Delta T_w^{*-n})^2/3 q(\kappa_{1/2})] + 4\sigma'_T \mathrm{Kn} T_w^{*-n}}$, where $\sigma'_T = \sigma'_{T_C}(1 + cN_\delta)$
E^2	$E_C^2 = \frac{(\gamma-1)}{8\alpha_{T_C}}\Pr M^2 \Delta_C^2$	$E_0^2 = \frac{(\gamma-1)}{8\alpha_{T_0}}\Pr M^2 \Delta_0^2$	$E^2 = \frac{(\gamma-1)}{8\alpha_T}\Pr M^2 \Delta^2$
$\frac{T}{T_w}$	$1 + E_C^2\left(1 - 4\alpha_{T_C} y^{*^2}\right)$	$1 + E_0^2\left(1 - 4\alpha_{T_0} s^{*^2}\right)$	$1 + E^2\left(1 - 4\alpha_T s^{*^2}\right)$
$\frac{\Pi_{xy}}{p(0)}$	$-N_\delta \Delta_C$	$-N_\delta \Delta_0 T_w^{*-n}$	$-\frac{q(\kappa_{1/2}) N_\delta \Delta T_w^{*-n}}{q^2(\kappa_{1/2}) + 2(N_\delta \Delta T_w^{*-n})^2/3}$
$\frac{\Pi_{yy}}{p(0)}$	0	0	$-\frac{2N_\delta^2 (\Delta T_w^{*-n})^2/3}{q^2(\kappa_{1/2}) + 2(N_\delta \Delta T_w^{*-n})^2/3}$; $\Pi_{zz} = \Pi_{yy}$ $\Pi_{xx} = -2\Pi_{yy}$
$\frac{Q_y}{p(0)V}$	$N_\delta \Delta_C^2 y^*$	$N_\delta \Delta_0^2 T_w^{*-n} s^*$	$\frac{q(\kappa_{1/2}) N_\delta \Delta^2 T_w^{*-n}}{q^2(\kappa_{1/2}) + 2(N_\delta \Delta T_w^{*-n})^2/3} s^*$
$\frac{Q_x}{p(0)V}$	0	0	$-\left(1 + \frac{1}{\Pr}\right)\frac{N_\delta^2 \Delta^3 T_w^{*-2n}}{[q^2(\kappa_{1/2}) + 2N_\delta^2 (\Delta T_w^{*-n})^2/3]} s^*$
y^* vs. s^*	$y^* = s^*$; temperature dependency ignored	$y^* = s^* T_w^* \left[1 + E_0^2\left(1 - \frac{4}{3}\alpha_{T_0} s^{*^2}\right)\right]$ for Maxwellian	$y^* = s^* T_w^* \left[1 + E^2\left(1 - \frac{4}{3}\alpha_T s^{*^2}\right)\right]$ for Maxwellian

$(T^{*^n} ds^* = dy^*, y^* \equiv y/h, T^* \equiv T/T_{ave}, N_\delta = \sqrt{2\gamma/\pi}\, M\ \mathrm{Kn})$.

With the nonlinear Smoluchowski temperature jump condition at wall surface (2.6),

$$T^*(s^* = 1/2) = T_w^* + \sigma'_T \mathrm{Kn} \frac{\Delta T}{T_r} Q_y^* \Big]_{s^*=1/2},\ \sigma'_T \equiv \frac{2\gamma}{\gamma+1}\frac{1}{\Pr}\sigma_T, \tag{3.26}$$

the temperature profile can be expressed as

$$T^*(s^*) = T^*(0) - 4\alpha_T \left[T^*(0) - T_w^*\right] s^{*2} \text{ and } T^*(0) = (1 + E^2) T_w^*, \tag{3.27}$$

where

$$\begin{aligned} E^2 &\equiv \frac{(\gamma-1)}{8\alpha_T}\Pr M^2 \Delta^2, \\ \alpha_T &\equiv \frac{1}{1 + 4\sigma'_T \mathrm{Kn} T_w^{*-n} \Pi^*/\Pi_0^*} = \frac{q(\kappa_{1/2}) + 2(N_\delta \Delta T_w^{*-n})^2/3 q(\kappa_{1/2})}{[q(\kappa_{1/2}) + 2(N_\delta \Delta T_w^{*-n})^2/3 q(\kappa_{1/2})] + 4\sigma'_T \mathrm{Kn} T_w^{*-n}}. \end{aligned} \tag{3.28}$$

From the equation of state, the density profile can also be determined as $\rho^* = T_w^*/T^*$. The temperature can be expressed in terms of E^2 and T_w^*,

TABLE II. Description of abnormal physical behaviors according to the second-order model.

Abnormal behaviors at high Knudsen number	Explanations based on the second-order model
Nonlinear velocity profile	The factor $1/T^{*^n}$, appearing in $du^*/dy^* = \Delta/T^{*^n}$, is the ultimate source of nonlinearity in the velocity profile, since $T^*(0)$ is always greater than $T^*(1/2)$, regardless of degree of non-equilibrium
Smaller velocity slip and shear stress	Through the nonlinearity of the constitutive relation (the shear-thinning property, that is, vanishing effective viscosity at high Knudsen number), $\Pi^*_{xy}/\Pi^*_{xy_0} = 3q(\kappa)/\left[3q^2(\kappa)+2\left(N_\delta \Pi^*_{xy_0}\right)^2\right]$, the second-order constitutive model predicts smaller shear stress in comparison with the first-order NSF model for a given strain rate at high non-equilibrium, allowing high velocity slope (or smaller velocity slip)
Velocity gradient singularity	The limiting behavior of velocity slope in the present theory; $\Delta/\Delta_C \to \infty$ as $\mathrm{Kn} \to \infty$, due to the slope limits $\lim_{N_\delta \to 0 \text{ or } \infty} \Delta \to 2\alpha_V (=2)$ from $\lim_{N_\delta \to 0 \text{ or } \infty} T^{*^n}_w q(c N_\delta)/N_\delta \to \infty$
Larger temperature difference	Combination of the shear-thinning property and the energy preservation in the cross-stream direction; $T(0) - T(1/2) = T_w(\gamma-1)\mathrm{Pr} M^2 \Delta^2/8$
Higher central temperature	Combination of the shear-thinning property and the dependence of the energy jump coefficient on N_δ through $\sigma_T = \sigma_{T_C}(1 + c N_\delta)$; $T(0)/T_w = (\gamma-1)\mathrm{Pr} M^2\Delta^2/\alpha_T/8$
Non-zero normal stress	Kinematic stress constraint embodied in the second-order model, $\Pi^2_{xy} = -3\left(p + \Pi_{yy}\right)\Pi_{yy}/2$, which represents the coupling of shear and normal stresses in the velocity shear flow
Relationship between primary and secondary normal stresses	Kinematic stress constraint embodied in the second-order model, $\Pi_{xx} = -2\Pi_{yy}$
Non-zero tangential heat flux	Non-Fourier law of heat flux embodied in the second-order model, $Q_x/Q_y = (1 + 1/\mathrm{Pr})\Pi_{xy}/(p + \Pi_{yy})$
Pronounced thermal effect	Two primary solutions (the velocity slope Δ and the average temperature T^*_w) are tightly interwoven at high Knudsen number through a cubic equation, $A\Delta^3 - 2\Delta^2 + 3\left[T^{*^n}_w q(\kappa_{1/2})/N_\delta\right]^2[\Delta/(2\alpha_V) - 1] = 0$

$$T^*(s^*) = T^*_w\left[1 + E^2\left(1 - 4\alpha_T s^{*^2}\right)\right]. \tag{3.29}$$

The unknown average temperature T^*_w can be determined by using the second equation in auxiliary relations (3.15); in the case of a Maxwellian molecule ($n = 1$), it is reduced to

$$T^*_w = \left[1 + E^2\left(1 - \frac{\alpha_T}{3}\right)\right]^{-1}. \tag{3.30}$$

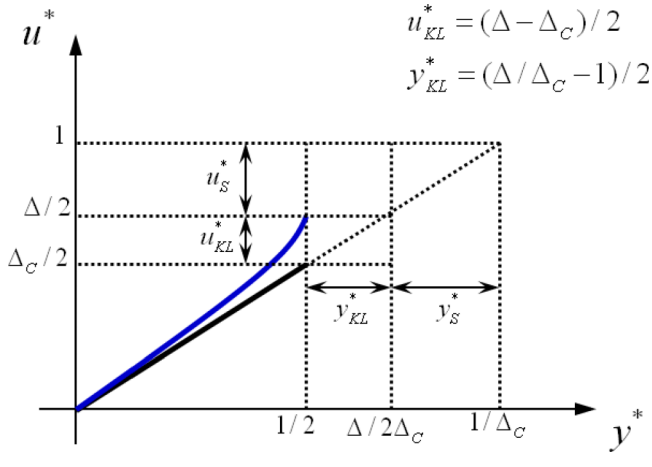

FIG. 4. Schematic of velocity field in the gaseous Knudsen layer.[1]

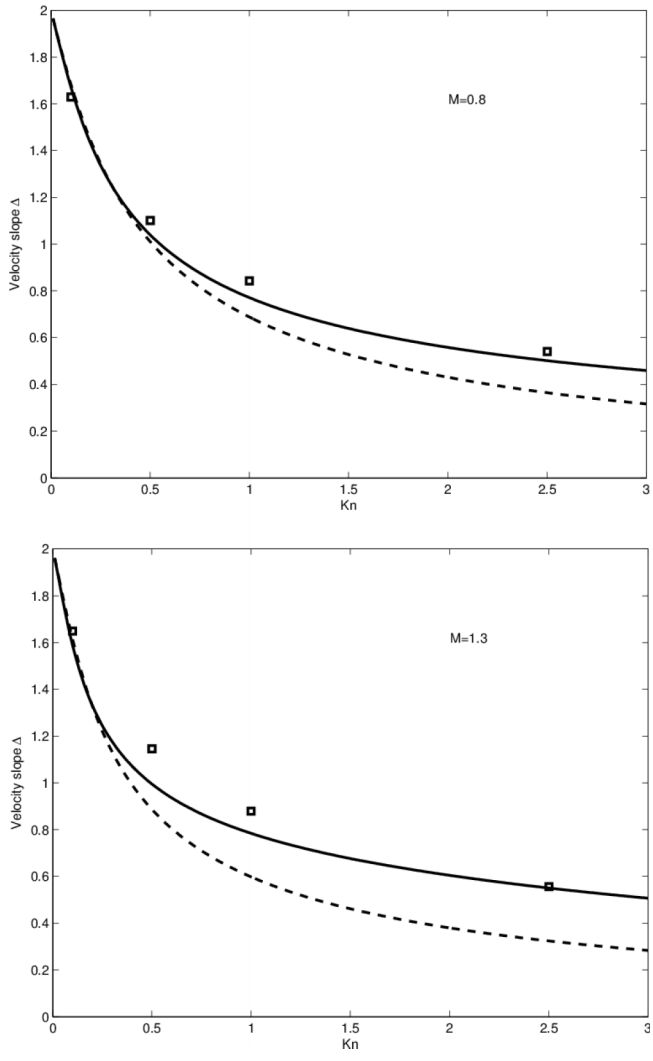

FIG. 5. The velocity slope Δ versus the Knudsen number in the plane Couette gas flow ($M = 0.8,\ 1.3, \sigma_{V_C} = 0.8, \sigma_{T_C} = 1.2$, Maxwellian). The solid line (—) represents results of the second-order theory, while the dotted line (– –) represents results of the Navier-Stokes-Fourier theory. The square symbols (□) represent the present DSMC results obtained by the Bird's Couette code.

Finally, the cumulant $\kappa_{1/2}$ appearing in (3.22), (3.23), and (3.20) can now be determined as

$$\kappa_{1/2} = cN_\delta\left[6\Pi^{*2}_{yy_{1/2}} + 2\Pi^{*2}_{xy_{1/2}} + \frac{2}{(\gamma-1)\,\mathrm{Pr}\,M^2}\frac{(\Delta T)^2}{T_r T_w}\frac{(Q^{*2}_{x_{1/2}} + Q^{*2}_{y_{1/2}})}{T^*_w\left[1+E^2(1-\alpha_T)\right]}\right]^{1/2} \quad \text{or}$$
$$\kappa_{1/2} = cN_\delta\left[6\Pi^{*2}_{yy_{1/2}} + 2\Pi^{*2}_{xy_{1/2}}\left[1 + \frac{(\gamma-1)\,\mathrm{Pr}\,M^2\Delta^2/4}{\left[1+E^2(1-\alpha_T)\right]}\left[1+\left(1+\frac{1}{\mathrm{Pr}}\right)\frac{N_\delta\Delta^2 T^{*-2n}_w}{q(\kappa_{1/2})}\right]\right]\right]^{1/2}. \tag{3.31}$$

In summary, Equations (3.22) and (3.30), with the help of (3.11), (3.16), (3.19), (3.20), (3.23), (3.28), and (3.31), comprise a system of nonlinear algebraic equations with dependent variables Δ and T^*_w. For initial data Kn and M, the system can be easily solved by a method of iterations. With these solutions, the slip velocity and the temperature jump can be determined from Equations (3.16) and (3.29), respectively. In addition, the relationships between s^* and y^* can be written as, in the

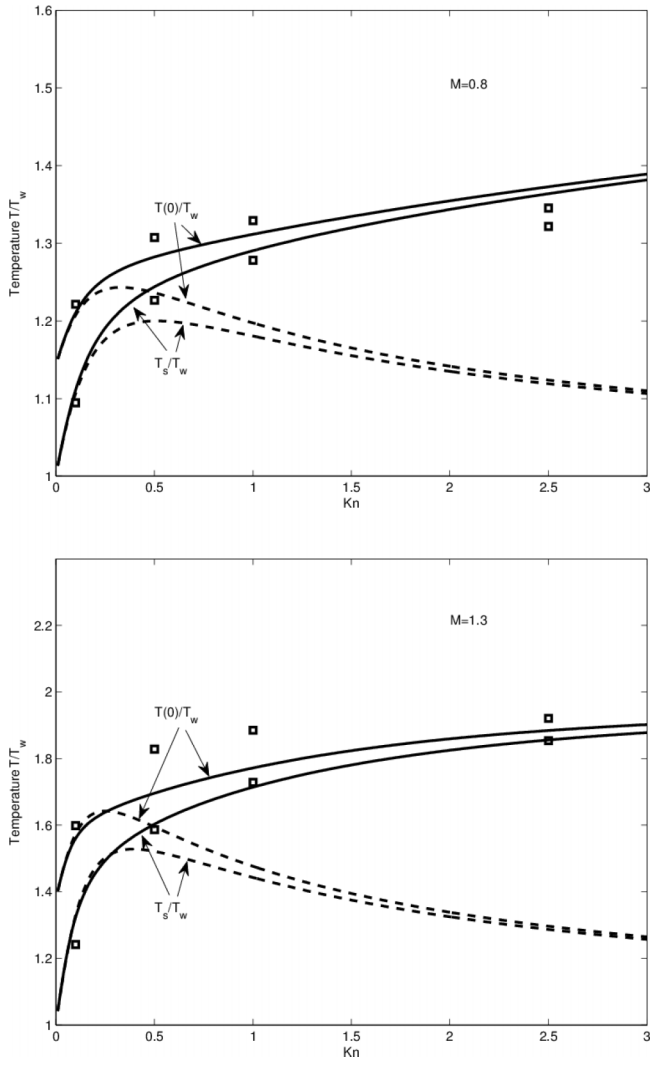

FIG. 6. Temperature T/T_w at center ($y^* = 0$) and wall ($y^* = \pm 1/2$) versus the Knudsen number in the plane Couette gas flow ($M = 0.8$, 1.3, $\sigma_{V_C} = 0.8$, $\sigma_{T_C} = 1.2$, Maxwellian). The solid lines (—) represent results of the second-order theory, while the dotted lines (– –) represent results of the Navier-Stokes-Fourier theory. The square symbols (□) represent the present DSMC results obtained by the Bird's Couette code.

case of a Maxwellian molecule ($n = 1$),

$$y^* = s^* T_w^* \left[1 + E^2\left(1 - \frac{4}{3}\alpha_T s^{*2}\right)\right] \text{ or}$$
$$s^* = \sqrt{\frac{1+E^2}{\alpha_T E^2}} \cos\left\{\frac{1}{3}\left[\cos^{-1}\left(-\frac{3}{T_w^*}\frac{\sqrt{\alpha_T}E}{(1+E^2)^{3/2}}y^*\right) + 4\pi\right]\right\}. \tag{3.32}$$

Also, the following relation can be further derived:

$$\frac{du^*}{dy^*} = \frac{\Delta}{T^*} = \frac{\Delta}{T_w^*\left[1 + E^2\left(1 - 4\alpha_T s^{*2}\right)\right]},$$
$$\frac{dT^*}{dy^*} = \frac{T_w^*\left(-8\alpha_T E^2 s^*\right)}{T^*} = -\frac{8\alpha_T E^2 s^*}{1 + E^2\left(1 - 4\alpha_T s^{*2}\right)}. \tag{3.33}$$

Analytical solutions of other cases such as $n = 1/2$ (hard sphere), $n = 3/4$, and $n = 4/5$ can be

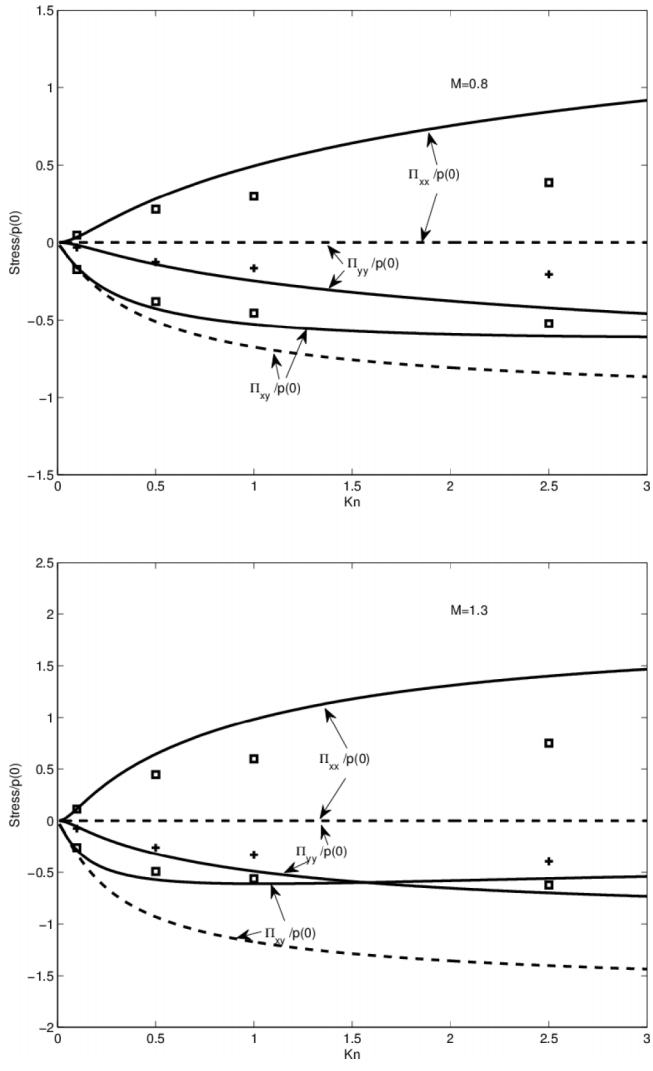

FIG. 7. Stress (shear and normal $\Pi_{xy,yy,xx}(y^*)/p(0)$) versus the Knudsen number in the plane Couette gas flow ($M = 0.8$, 1.3, $\sigma_{V_C} = 0.8$, $\sigma_{T_C} = 1.2$, Maxwellian). The solid lines (—) represent results of the second-order theory, while the dotted lines (– –) represent results of the Navier-Stokes-Fourier theory. The square (□) and plus (+) symbols represent the present DSMC results obtained by the Bird's Couette code.

deduced from expressions in Appendix C with new definition of quantities Δ, E, α_T given in (3.22) and (3.28) in place of $\Delta_0, E_0, \alpha_{T_0}$.

IV. RESULTS AND DISCUSSIONS: NON-CLASSICAL AND NON-ISOTHERMAL EFFECTS ACCORDING TO THE SECOND-ORDER MODELS

A complete set of analytical solutions to the gaseous Couette flow, (3.2), (3.3), (3.8), and (3.16)-(3.33), is obtained by new theory based on the second-order NCCR and velocity slip and temperature jump models. The construction of a unique flow solution for the given physical conditions specified in terms of Mach and Knudsen numbers is illustrated in Fig. 3. The existence of an analytical solution for the physical conditions ($0 \leqslant M < \infty$ and $0 < \mathrm{Kn} < \infty$) has been shown through cubic algebraic equation (3.22). Note that not only is the velocity slope $(\eta/\eta_w)du/dy$ a primary solution, but the average temperature T_{ave} (or T_r) is also. It must also be reiterated that, owing to the algebraic nature of the second-order NCCR model in the present shear dominated flow, no additional boundary conditions beyond the usual velocity slip and temperature jump are necessary in the present theory. Once two primary solutions (Δ, T_w^*) are obtained, the central properties

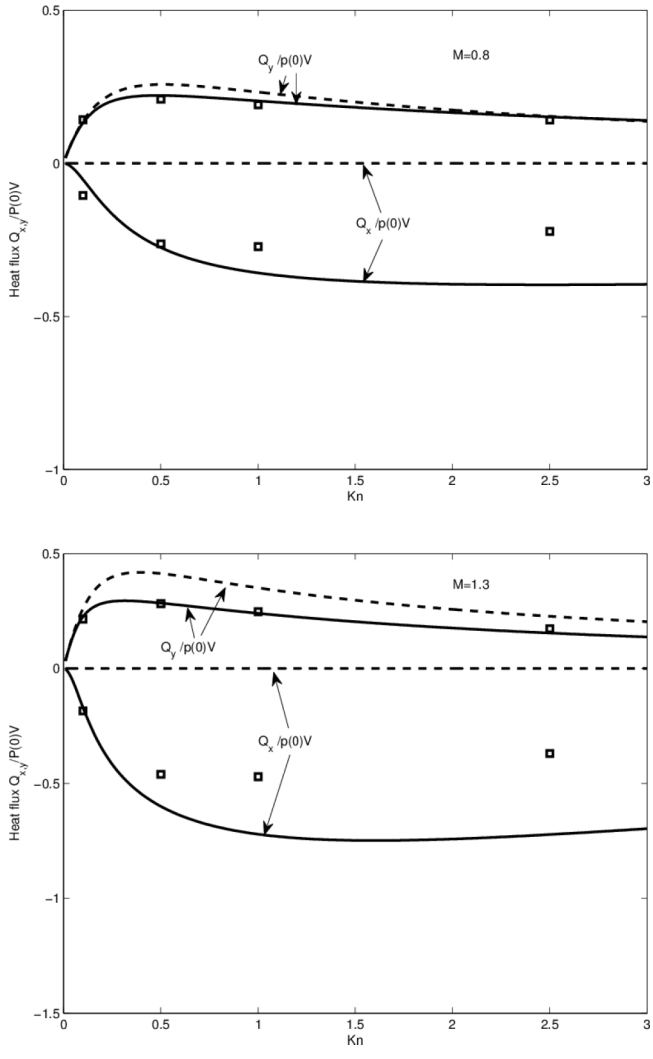

FIG. 8. Heat flux (normal and tangential $Q_{y,x}(y^*)/p(0)V$) versus the Knudsen number in the plane Couette gas flow ($M = 0.8$, 1.3, $\sigma_{V_C} = 0.8$, $\sigma_{T_C} = 1.2$, Maxwellian). The solid lines (—) represent results of the second-order theory, while the dotted lines (– –) represent results of the Navier-Stokes-Fourier theory. The square symbols (□) represent the present DSMC results obtained by the Bird's Couette code.

$T(0), \rho(0)$ follow. Consequently, all other analytical solutions for conserved and non-conserved variables can be obtained, as summarized in Table I.

The underlying mechanisms behind the abnormal properties in the Knudsen layer in Couette flow may be explained by these analytical solutions in a concise way. A summary of the physical description of abnormal behaviors according to the new theory is given in Table II. Among several intriguing non-classical behaviors, the nonlinear velocity profile has been the center of extensive study. A close examination of the velocity profiles in Table I reveals that the factor $1/T^{*^n}$, appearing in $du^*/dy^* = \Delta/T^{*^n}$, is the ultimate source of nonlinearity in the velocity profile. Since $T^{*^n}(1/2) < T^{*^n}(0)$, regardless of degree of non-equilibrium, in the present Couette flow, $du^*/dy^*(1/2)$ is always greater than $du^*/dy^*(0)$, resulting in the nonlinear velocity profile illustrated in Fig. 4. Furthermore, it can be observed from the y^* and s^* relationship that the nonlinearity is enhanced for high Mach number flow.

A similar rationale can be applied to the explanation of another abnormal behavior, that is, smaller velocity slip and shear stress at high Knudsen numbers. As shown in Fig. 5, the velocity at the wall $\Delta/2$ (or the velocity slope Δ) becomes larger at high Knudsen numbers in comparison

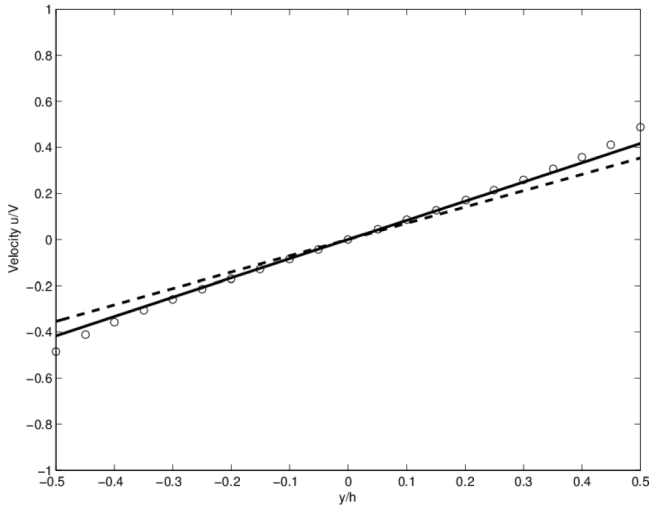

FIG. 9. Velocity profile $u(y^*)/V$ in the plane Couette gas flow ($M = 1.0$, Kn = 1.0; $\sigma_{V_C} = 0.8$, $\sigma_{T_C} = 1.2$, hard sphere). The solid line (—) and (○) symbols represent results of the second-order theory and DSMC method (Lockerby and Reese[22]), respectively, while the dotted line (– –) represents results of the Navier-Stokes-Fourier theory.

with that of the Navier-Stokes-Fourier theory $\Delta_0/2 = \alpha_{V_0}$, resulting in a smaller velocity slip, which is also illustrated in Fig. 4. The ultimate origin of this property is the nonlinearity of the constitutive relation for shear stress contained in the second-order NCCR model, for example, relation (D1) of Appendix D in a BGK[48] approximation (for details, refer to Figure 2 in the work of Myong[39]). The second-order NCCR model predicts smaller shear stress for a given strain rate at high non-equilibrium, allowing high velocity slope (or smaller velocity slip) in the present Couette flow. This simple description is made possible by a judicious combination with the nonlinear Maxwell velocity slip condition through the term $\Pi^*(y^* = 1/2)$. With this crucial step, the nonlinearity of the second-order NCCR model is morphed into the determination of the velocity slip through the cubic equation of velocity slope (3.22), specifically, through the term $(A\Delta^3 - 2\Delta^2)(N_\delta T_w^{*-n}/q(\kappa_{1/2})^2$. This term plays a negligible role near equilibrium (small N_δ), but it dominates at high non-equilibrium, resulting in increasing Δ/Δ_0 for finite large N_δ, and ultimately the velocity gradient singularity at infinite N_δ.

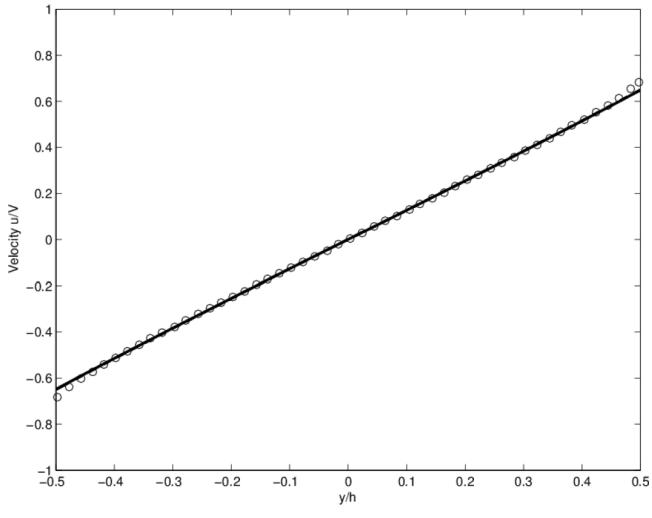

FIG. 10. Velocity profile $u(y^*)/V$ in the plane Couette gas flow ($M = 1.0$, Kn = 0.25; $\sigma_{V_C} = 0.8$, $\sigma_{T_C} = 1.2$, hard sphere). The solid line (—) and (○) symbols represent results of the second-order theory and DSMC method (Marques and Kremer[10]), respectively, while the dotted line (– –) represents results of the Navier-Stokes-Fourier theory.

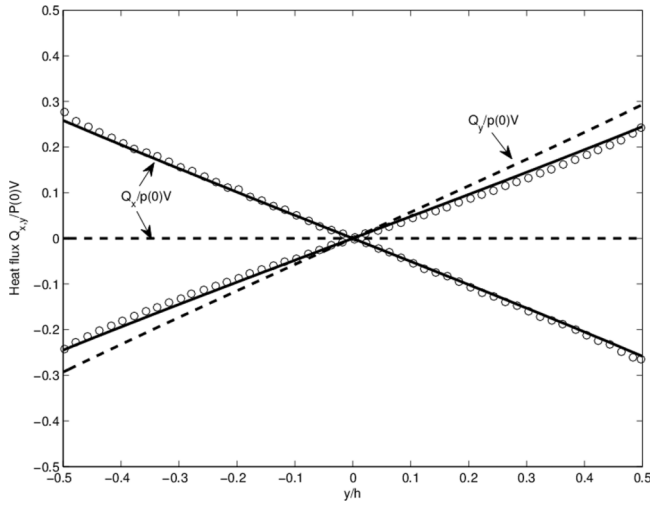

FIG. 11. Heat flux profile $Q_{y,x}(y^*)/p(0)V$ in the plane Couette gas flow ($M = 1.0$, Kn = 0.25; $\sigma_{V_C} = 0.8$, $\sigma_{T_C} = 1.2$, hard sphere). The solid lines (—) and (○) symbols represent results of the second-order theory and DSMC method (Marques and Kremer[10]), respectively, while the dotted lines (– –) represent results of the Navier-Stokes-Fourier theory.

This rather benign behavior may also explain, within the continuum framework, the mechanism behind the velocity gradient singularity in the Knudsen layer, which was investigated extensively by Lilley and Sader[18] using the DSMC method; such a singularity is reflected as a limiting behavior, $\Delta/\Delta_0 \to \infty$ as $\mathrm{Kn} \to \infty$, due to the slope limits $\lim_{N_\delta \to \infty} \Delta \to 2\alpha_V (= 2)$ from $\lim_{N_\delta \to \infty} T_w^{*n} q(cN_\delta)/N_\delta \to \infty$, in the present theory.

In order to validate the abnormal physical behaviors according to the new second-order theory in various regimes, DSMC solutions are obtained by using the Bird's Couette code[49] with the diffusive wall condition, because DSMC results are believed to be qualitatively accurate in general if the values of computational parameters (time-step, cell-size, and the number of particles) are chosen properly.[50] The total number of molecules in the system was set as 1.4×10^{20}, while the size (height) of channel was varied with depending on Knudsen numbers. The number of cells is 200 across the channel, and the simulation time step is selected as 2.5×10^{-6} s. In the case of continuum theories, adjustable parameters of the velocity slip and temperature jump constants—chosen

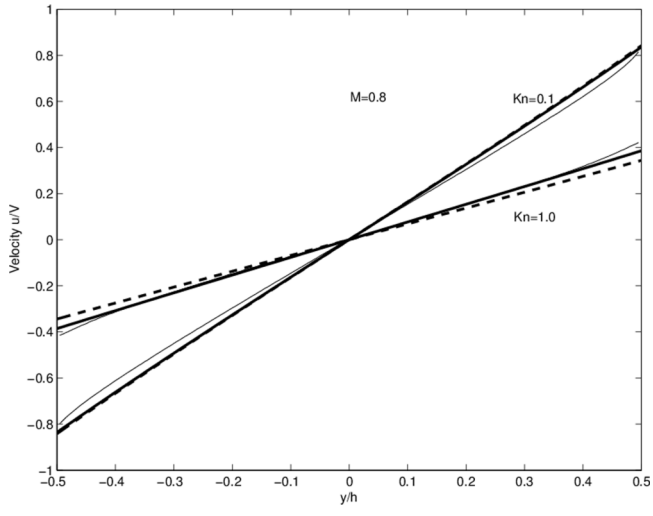

FIG. 12. Velocity profile $u(y^*)/V$ in the plane Couette gas flow ($M = 0.8$, Kn = 0.1, 1.0; $\sigma_{V_C} = 0.8$, $\sigma_{T_C} = 1.2$, Maxwellian). The thick solid lines (—) represent results of the second-order theory, while the dotted lines (– –) represent results of the Navier-Stokes-Fourier theory. The thin solid lines (—) represent the present DSMC results obtained by the Bird's Couette code.

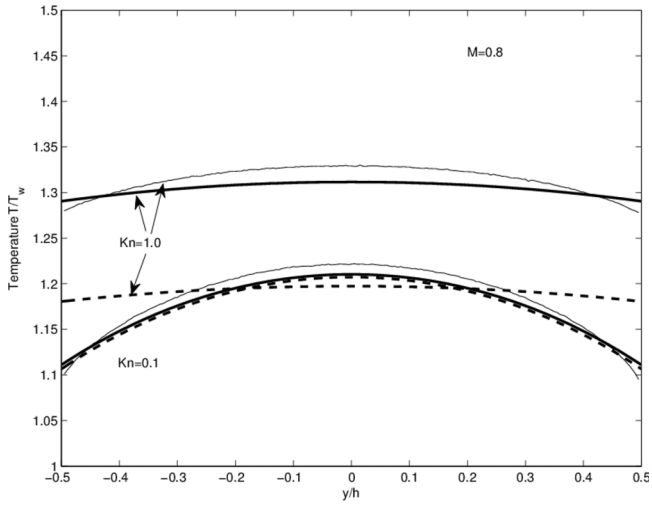

FIG. 13. Temperature profile $T(y^*)/T_w$ in the plane Couette gas flow ($M = 0.8$, Kn = 0.1, 1.0; $\sigma_{V_C} = 0.8$, $\sigma_{T_C} = 1.2$, Maxwellian). The thick solid lines (—) represent results of the second-order theory, while the dotted lines (– –) represent results of the Navier-Stokes-Fourier theory. The thin solid lines (—) represent the present DSMC results obtained by the Bird's Couette code.

as best fit for the DSMC results—are assumed $\sigma_{V_C} = 0.8$, $\sigma_{T_C} = 1.2$ throughout for both of the Navier-Stokes-Fourier and second-order theories.

As shown in Fig. 5, the velocity slope for a given Mach number decreases with respect to the Knudsen number in the transition regimes, but the velocity slope of the second-order theory (and the DSMC solutions of different Knudsen numbers 0.1, 0.5, 1.0, and 2.5) remains greater than that of the Navier-Stokes-Fourier theory with varying coefficients and the difference increases with increasing Knudsen numbers, ultimately yielding the velocity gradient singularity. The ultimate reason behind this behavior is the shear-thinning property, that is, vanishing effective viscosity at high Knudsen number, embodied in the second-order constitutive relation.

Furthermore, the shear-thinning property of the second-order NCCR model may explain the larger difference between the temperature at the center and near the wall, observed from DSMC results. From the analytical solutions in Table I, it can be noted that a simple relation exists between temperature difference and the velocity slope: $T(0) - T(1/2) = T_w(\gamma - 1)\,\mathrm{Pr}\,M^2\Delta^2/8$. Thus, higher velocity slope (or smaller velocity slip) at high Knudsen numbers is directly related to the larger temperature difference for a given Mach number, as illustrated in Fig. 6. Moreover, it can be noted that the temperature in the second-order NCCR theory (and the DSMC solutions) behaves qualitatively different from that of the Navier-Stokes-Fourier theory from the transition regime (around Knudsen number 0.25) and beyond, monotonic increase versus decrease. The reason behind this difference was found to be the dependence of the energy jump coefficient on the degree of non-equilibrium through $\sigma_T = \sigma_{T_C}(1 + cN_\delta)$ in the second-order temperature jump condition. With this crucial element, the second-order NCCR theory is able to describe the non-isothermal effects of the Knudsen layer in qualitative agreement with the DSMC solutions.

According to the new theory illustrated in Figs. 7 and 8, it is also shown that non-zero normal stresses and tangential heat flux appear in states away from thermal equilibrium in qualitative agreement with the DSMC results, including the correct relationship between primary and secondary stresses, $\Pi_{yy} = -\Pi_{xx}/2$. Note that the first-order Navier-Stokes-Fourier theory cannot describe the existence of the non-zero normal stresses and tangential heat flux at all. The existence of non-zero normal stresses according to the second-order theory can be easily explained by kinematic stress constraints (3.3) and (3.5), which represent the coupling of shear and normal stresses in the velocity shear flow. On the other hand, the origin of non-zero tangential heat flux may be explained in the present theory by non-Fourier laws (3.6) and (3.11).

In order to further compare the new theory with the DSMC results available in the literature, three cases, $M = 1.0$, Kn = 1.0 for a hard sphere gas ($\Delta/2 = 0.354$ and 0.417, $T_w^* = 0.767$ and

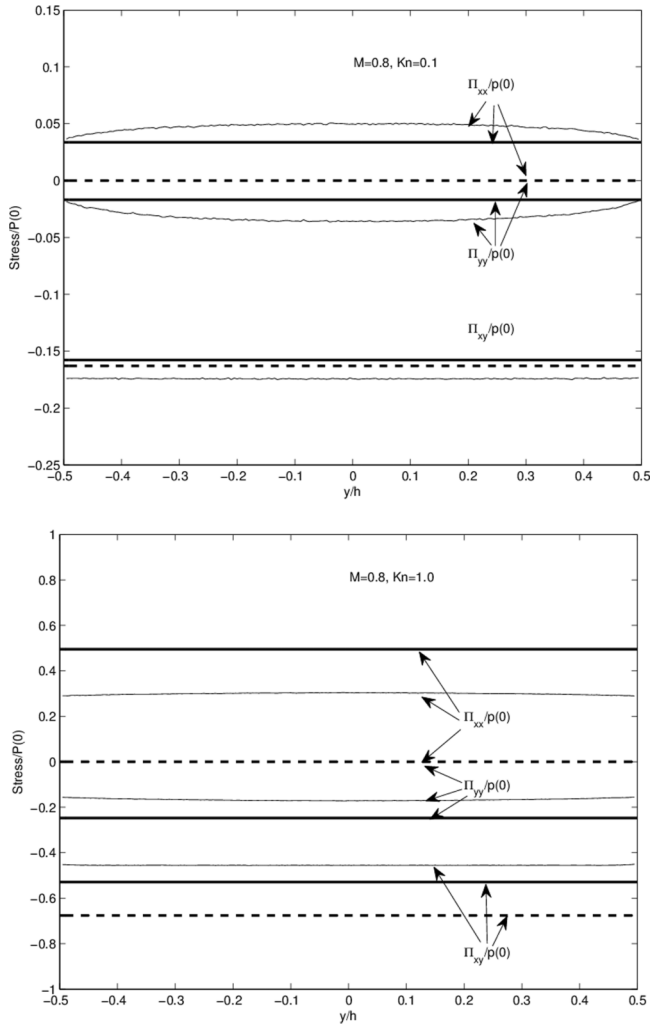

FIG. 14. Viscous stress profile (shear and normal $\Pi_{xy,yy,xx}(y^*)/p(0)$) in the plane Couette gas flow ($M = 0.8$, Kn = 0.1, 1.0; $\sigma_{V_C} = 0.8$, $\sigma_{T_C} = 1.2$, Maxwellian). The thick solid lines (—) represent results of the second-order theory, while the dotted lines (– –) represent results of the Navier-Stokes-Fourier theory. The thin solid lines (—) represent the present DSMC results obtained by the Bird's Couette code.

0.654, in case of NSF and NCCR solutions, respectively), reported by Lockerby and Reese;[22] M = 1.0, Kn = 0.25 for a Maxwellian molecule ($\Delta/2 = 0.65$ and 0.648, $T_w^* = 0.742$ and 0.734, in case of NSF and NCCR solutions, respectively), calculated by Marques and Kremer;[10] and M = 0.8, Kn = 0.1, 1.0 for a Maxwellian molecule ($\Delta/2 = 0.842$ and 0.836 for Kn = 0.1 and 0.344 and 0.386 for Kn = 1.0, $T_w^* = 0.852$ and 0.849 for Kn = 0.1, 0.839 and 0.767 for Kn = 1.0, in case of NSF and NCCR solutions, respectively), studied by Thatcher[13] and Ejtehadi *et al.*,[51] are chosen. The adjustable velocity slip and temperature jump constants are again assumed $\sigma_{V_C} = 0.8$, $\sigma_{T_C} = 1.2$ throughout for both of the Navier-Stokes-Fourier and second-order theories.

In Fig. 9, the dimensionless velocity profiles are depicted with regard to the location y^*. In this high Knudsen number case, the second-order NCCR theory differs significantly from the Navier-Stokes-Fourier theory and is in strong qualitative agreement with the DSMC prediction, in particular regarding the smaller velocity slip at the wall. In the smaller Knudsen number (Kn = 0.25) case, the difference in velocity profile with the linear theory is significantly reduced, almost indistinguishable, as shown in Fig. 10. The normal and tangential heat flux profiles are also depicted in Fig. 11. Both first-order and second-order NCCR theories predict normal heat flux

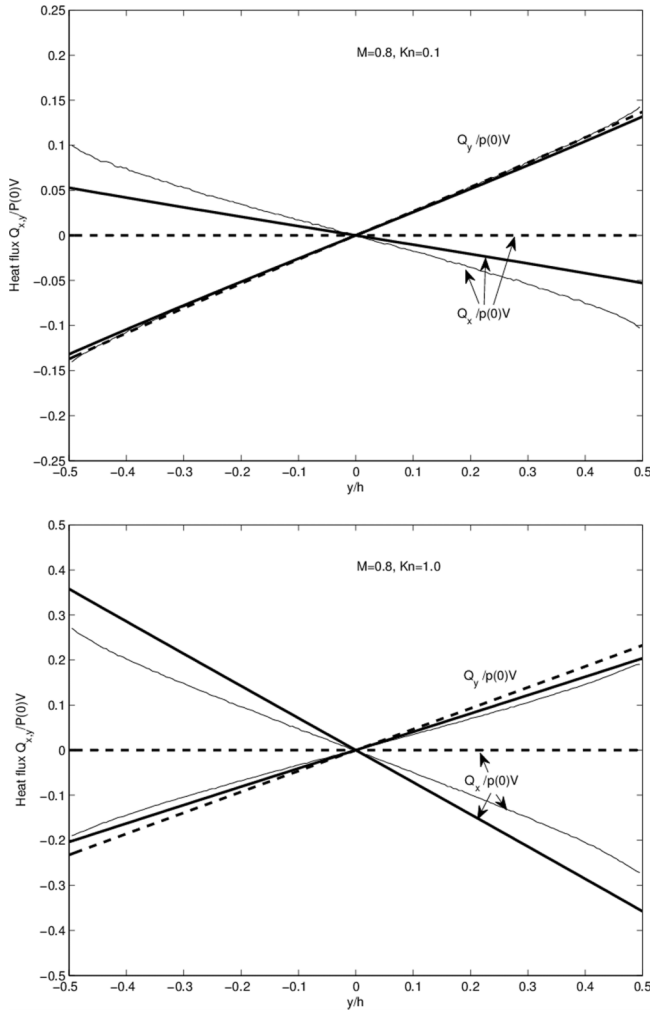

FIG. 15. Heat flux profile $Q_{y,x}(y^*)/p(0)V$ in the plane Couette gas flow ($M = 0.8$, Kn = 0.1, 1.0; $\sigma_{V_C} = 0.8$, $\sigma_{T_C} = 1.2$, Maxwellian). The thick solid lines (—) represent results of the second-order theory, while the dotted lines (– –) represent results of the Navier-Stokes-Fourier theory. The thin solid lines (—) represent the present DSMC results obtained by the Bird's Couette code.

in close agreement with the DSMC results, while only the second-order NCCR theory is able to predict the tangential heat flux in qualitative agreement with the DSMC results.

Similar results can be found in another case ($M = 0.8$, Kn = 0.1, 1.0), as illustrated in Figs. 12-15 that show the actual profiles of the present DSMC solutions in Figs. 5-8 obtained by using the Bird's Couette code. In Fig. 12, the nonlinearity of the velocity profile is clearly visible in the second-order theory, in the higher slope near the wall in comparison with that at the center. The DSMC results also show the nonlinearity and its level is enhanced in comparison with the continuum theories. This difference in the nonlinearity level is suspected due to the gap between the strict uniform pressure of the second-order solution and the non-uniform pressure property of the DSMC solution. It is worth to mention that the constant pressure was also found in the solution of the infinite hierarchy of moment equations derived from the Boltzmann equation for Maxwell molecules in the case of steady Couette flow.[52,53] Therefore, it is expected that the gap will be reduced once the strict uniform pressure is enforced in the DSMC Couette code.

On the other hand, there exists a qualitative difference for the temperature profile between the first-order theory and the second-order theory, as shown in Fig. 13. As already explained in Fig. 6, the temperature in the second-order NCCR theory (and the DSMC solutions) behaves qualitatively

different from that of the Navier-Stokes-Fourier theory in the transition regime with Knudsen number 1.0. The higher temperature in the second-order solution, $T(0)/T_w = (\gamma - 1)\,\mathrm{Pr}\,M^2\Delta^2/\alpha_T/8$, is directly related to the linear dependence of the energy jump coefficient on the degree of non-equilibrium N_δ in the second-order temperature jump condition of α_T.

Fig. 14 shows the viscous stresses including non-classical second-order effects: non-zero normal (primary and secondary) stresses in states away from thermal equilibrium. The second-order NCCR solutions in these transition regimes are in strong qualitative agreement with the DSMC results for all aspects, while the first-order Navier-Stokes-Fourier theory describes none of these abnormal properties. In particular, the relationship between primary and secondary stresses, $\Pi_{yy} = -\Pi_{xx}/2$, is clearly demonstrated in Fig. 14. Note also that the DSMC results show some degree of non-uniformity in the profiles of normal (primary and secondary) stresses, while they show strict uniformity in the profile of the shear stress. Again, the reason behind this disparity of the DSMC results is due to the fact that the strict uniform pressure is not enforced in the DSMC Couette code.

Fig. 15 shows the heat fluxes including the non-classical second-order tangential heat flux in states away from thermal equilibrium. Again, the second-order NCCR solutions of heat fluxes are in strong qualitative agreement with the DSMC results, while the first-order Navier-Stokes-Fourier theory cannot describe the non-classical tangential heat flux. Overall, the present second-order NCCR and slip and jump models capture all the qualitative features in transition regimes predicted by the DSMC method: nonlinear velocity, smaller velocity slip, higher central temperature, non-zero normal stresses, direct relationship between primary and secondary normal stresses, and non-zero tangential heat flux.

V. CONCLUDING REMARKS

Non-classical and non-isothermal effects on the gaseous Couette flow in thermal non-equilibrium (equivalently, the gaseous Knudsen layer near a solid surface through a transform into the reference frame of Kramers' problem using a proper coordinate change) are explained by developing a complete set of analytical solutions on the basis of the second-order constitutive and velocity slip and temperature jump models. The main features of the theory are the implicit exponential sinh form $q(cN_\delta)/N_\delta$ in the second-order constitutive relation and the dependence of the temperature jump coefficient on the degree of non-equilibrium through $\sigma_T = \sigma_{T_C}(1 + cN_\delta)$ in the second-order temperature jump condition. According to the new second-order theory, as summarized in Table II, the smaller velocity slip and shear stress are shown to arise due to the non-Navier shear-thinning property of the second-order NCCR model, that is, vanishing effective viscosity at high Knudsen number. Also, the non-zero normal stress and tangential heat flux are caused by the kinematic stress constraint and non-Fourier law of heat flux embodied in the second-order NCCR model, respectively.

The present analytical solutions are self-contained in the sense that no adjustment using external information from more accurate results like kinetic theories is needed. This was not the case in most previous studies where the shear rate was determined from an external source, for example, the DSMC method. It is also demonstrated that the second-order NCCR model in implicit algebraic form, interwoven with the nonlinear coupled wall boundary model, is just enough to explain qualitatively all the known properties of the Knudsen layer predicted by the DSMC. In particular, when the shear-thinning property of the second-order constitutive model is morphed into the determination of the velocity slip in the nonlinear slip and jump model, the new second-order continuum theory predicts smaller shear stress for a given strain rate at high non-equilibrium, leading to high velocity slope and ultimately the velocity gradient singularity with the power law dependence. This capability may be considered an important step toward paving the way for developing accurate higher-order continuum models more easily applicable for problems of practical interest that have complex geometry. The reason is that the *algebraic* constitutive equation circumvents the burden of developing additional boundary conditions for higher-order moments (shear stress and heat flux) arising in the traditional *partial differential* constitutive equations.

One of the basic tenets used in this study is mathematical technique (3.12)-(3.15), that is, the introduction of dimensionless variables and average temperature and a variable scaled by the temperature. Through this technique, temperature variation of viscosity and thermal conductivity coefficients was treated in a rigorous way and, thereby, the non-isothermal effects in the gaseous Knudsen layer in Couette flow were elucidated in detail. Furthermore, such a technique enabled the property at the center to be determined precisely as a part of the solutions. This tenet, together with the second-order constitutive and velocity slip and temperature jump models, may be carried again over to the more challenging *pressure-driven* Poiseuille gas flow, which is another important problem in rarefied and microscale gases. The result of the investigation of the problem from the framework developed here will be reported in due course.

ACKNOWLEDGMENTS

This work was supported by the National Research Foundation of Korea funded by the Ministry of Education, Science and Technology (NRF Nos. 2015-M1A3A3A02-010621 and 2012-R1A2A2A02-046270), South Korea. The author gratefully acknowledges the help of Abolfazl Karchani for producing the present DSMC results using the Bird's Couette code. He also thanks the referees of this paper for their valuable and very helpful comments.

APPENDIX A: SOLUTIONS OF NAVIER-STOKES-FOURIER EQUATIONS WITH CONSTANT COEFFICIENTS

When the classical constitutive relations by Navier-Stokes and Fourier are combined with the conservation laws, the governing equation of gaseous Couette flow (3.1) is reduced to the following system of ordinary differential equations:

$$\frac{d}{dy}\begin{bmatrix}\Pi_{xy}\\ p+\Pi_{yy}\\ \Pi_{yz}\\ \Pi_{xy}u+Q_y\end{bmatrix}=\begin{bmatrix}0\\0\\0\\0\end{bmatrix},\quad \begin{bmatrix}\Pi_{yy}\\ \Pi_{xy}\\ \Pi_{yz}\\ Q_x\\ Q_y\end{bmatrix}=\begin{bmatrix}0\\ -\eta du/dy\\ 0\\ 0\\ -kdT/dy\end{bmatrix}. \tag{A1}$$

The combination of the second and fifth equations yields the uniform pressure distribution $p = p(y = 0)$. It is also obvious that $\Pi_{xx} = \Pi_{zz} = \Pi_{xz} = Q_x = Q_z = 0$. The system is then simplified into differential equations with unknowns of the stream-wise velocity u and the temperature T only,

$$\frac{d}{dy}\begin{bmatrix}\Pi_{xy}\\ \Pi_{xy}u+Q_y\end{bmatrix}=\begin{bmatrix}0\\0\end{bmatrix},\quad \begin{bmatrix}\Pi_{xy}\\ Q_y\end{bmatrix}=\begin{bmatrix}-\eta du/dy\\ -kdT/dy\end{bmatrix}. \tag{A2}$$

Then, the velocity solution in the function of the distance y can be determined by solving the x-momentum equation with the Navier-Stokes law

$$\frac{d}{dy}\left(-\eta\frac{du}{dy}\right)=0 \text{ or constant } \Pi_{xy}\left(\equiv -\eta\frac{du}{dy}\right)=\Pi_C, \tag{A3}$$

where the subscript C denotes the Navier-Stokes-Fourier theory with constant coefficients. With the assumption of *constant* viscosity, the *linear* velocity profile is then derived as follows:

$$u(y)=-\frac{\Pi_C}{\eta}y. \tag{A4}$$

Here, a condition at the centerline owing to the anti-symmetric nature of the velocity profile has been applied, $u(0) = 0$. With first-order Maxwell slip boundary condition (2.5),

$$u\left(y=\frac{h}{2}\right)=V-\sigma_{V_C}l\left.\frac{du}{dy}\right]_{y=h/2}, \tag{A5}$$

the shear stress in Equation (A3) can be determined as (velocity slope $\Delta_C \equiv du^*/dy^*$)

$$\Delta_C = 2\alpha_{V_C} = -\frac{\Pi_C}{\eta V/h}. \tag{A6}$$

Here, a dimensionless number α_{V_C}, the Knudsen number, and the mean free path are defined as

$$\alpha_{V_C} \equiv \frac{1}{1+2\sigma_{V_C}\mathrm{Kn}}, \quad \mathrm{Kn} \equiv \frac{l}{h} = \sqrt{\frac{\pi}{2}}\frac{\eta\sqrt{RT_w}}{ph}, \quad l = \sqrt{\frac{\pi}{2}}\frac{\eta\sqrt{RT_w}}{p}.$$

The temperature profile can be obtained by solving the momentum and energy equations in the conservation laws. The resulting equation reduces to

$$\frac{dQ_y}{dy} = \frac{\Pi_C^2}{\eta}. \tag{A7}$$

When this is integrated once with respect to y, the heat flux in the y-direction can be written as

$$Q_y = \frac{\Pi_C^2}{\eta} y. \tag{A8}$$

Here, a condition at the centerline has been applied, $Q_y(0) = 0$. With the Fourier law and the assumption of *constant* thermal conductivity, the following temperature profile can be determined:

$$T(y) = T(0) - \frac{h^2\Pi_C^2}{2\eta k}(y/h)^2. \tag{A9}$$

With the first-order Smoluchowski temperature jump at wall surface Eq. (2.5),

$$T\left(y = \frac{h}{2}\right) = T_w - \sigma'_{T_C} l \left.\frac{dT}{dy}\right]_{y=h/2}, \tag{A10}$$

the temperature profile can be expressed as

$$T(y) = T(0) - 4\alpha_{T_C}\left[T(0) - T_w\right](y/h)^2 \text{ and } \frac{h^2\Pi_C^2}{8\eta k} = \alpha_{T_C}\left[T(0) - T_w\right], \tag{A11}$$

where

$$\alpha_{T_C} \equiv \frac{1}{1+4\sigma'_{T_C}\mathrm{Kn}}.$$

For this *quadratic* profile, the average temperature can be easily calculated as

$$T_{ave} \equiv \frac{\int_0^{h/2} T dy}{h/2} = T_w + \frac{h^2\Pi_C^2}{8\eta k}\frac{3-\alpha_{T_C}}{3\alpha_{T_C}} \text{ or } \frac{T_w}{T_{ave}} = \left(1 + \frac{h^2\Pi_C^2}{8\eta k T_w}\frac{3-\alpha_{T_C}}{3\alpha_{T_C}}\right)^{-1}. \tag{A12}$$

It should be mentioned that the average temperature can be defined differently, for example, $T_r = \left[\int_0^{h/2} 1/T dy\right]^{-1}(h/2)$ like (3.13), but the final solutions will remain exactly the same. Note that the value T_{ave} is well-defined for all the physical conditions of Π_C, h and is always greater than the wall temperature T_w. When it is combined with relation (A11), the centerline temperature, *which itself is the part of solution*, can be determined as

$$T(0) = \frac{3T_{ave} - \alpha_{T_C}T_w}{3-\alpha_{T_C}}. \tag{A13}$$

It should be mentioned that, *as far as the present author is aware of, the precise form of the central temperature* $T(0)$ *has never been reported in the past*. Note that the value $T(0)$ is well-defined for all the physical conditions. With the introduction of a positive quantity E_C, determined solely by initial conditions $M(\equiv V/\sqrt{\gamma RT_w})$ and Kn,

$$E_C^2 \equiv \frac{h^2\Pi_C^2}{8\alpha_{T_C}\eta k T_w} = \frac{(\gamma-1)}{8\alpha_{T_C}}\mathrm{Pr}\, M^2\Delta_C^2,$$

the temperature and its average reduce to

$$\frac{T(y)}{T_w} = 1 + E_C^2\left[1 - 4\alpha_{T_C}\left(\frac{y}{h}\right)^2\right], \quad \frac{T_w}{T_{ave}} = \left[1 + E_C^2\left(1 - \frac{\alpha_{T_C}}{3}\right)\right]^{-1}. \tag{A14}$$

APPENDIX B: SOLUTIONS OF NAVIER-STOKES-FOURIER RELATIONS WITH VARYING COEFFICIENTS

When the Navier-Stokes-Fourier relations with varying coefficients are considered, the system of ordinary differential equations with dependent variables u and T may first be solved in terms of the variable s; the solutions are later expressed in the function of the distance y. The x-momentum equation in (A2) is then reduced as follows:

$$\text{constant } \Pi_{xy}\left(\equiv -\eta\frac{du}{dy}\right) = \Pi_0, \tag{B1}$$

where the subscript 0 denotes the Navier-Stokes-Fourier theory with varying coefficients. With the introduction of viscosity $\eta(T) = \eta_w(T/T_w)^n$, the momentum equation can be written as

$$\Pi_0^* = -\frac{1}{T_w^{*n}}\frac{du^*}{ds^*} \tag{B2}$$

and, after an integration, the following velocity profile can be derived:

$$u^*(s^*) = \Delta_0 s^*, \tag{B3}$$

where

$$\Delta_0\left(\equiv \frac{du^*}{ds^*}\right) = -\Pi_0^* T_w^{*n}.$$

With first-order Maxwell slip boundary condition (2.5),

$$u^*(y^* = 1/2) = 1 - \sigma_{V_C}\mathrm{Kn}\left.\frac{du^*}{dy^*}\right]_{y^*=1/2} \text{ or } u^*(s^* = 1/2) = 1 - \sigma_{V_C}\mathrm{Kn}T_w^{*-n}\left.\frac{du^*}{ds^*}\right]_{s^*=1/2}, \tag{B4}$$

the shear stress Π_0^* (or the velocity slope Δ_0) in Equation (B3) can be determined as

$$\Delta_0 = -\Pi_0^* T_w^{*n} = 2\alpha_{V_0}, \tag{B5}$$

where

$$\alpha_{V_0} \equiv \frac{1}{1 + 2\sigma_{V_C}\mathrm{Kn}T_w^{*-n}}.$$

With introduction of thermal conductivity $k(T) = k_w(T/T_w)^n$, the energy equation is reduced to

$$\frac{dQ_y^*}{ds^*} = \mathrm{Pr}\,\mathrm{Ec}T_w^{*n}\Pi_0^{*2}. \tag{B6}$$

When it is integrated once with respect to s^*, the heat flux in the y-direction can be written as

$$Q_y^* = \mathrm{Pr}\,\mathrm{Ec}\Pi_0^*(-\Delta_0)s^* \text{ or } \frac{Q_y}{pV} = N_\delta\Pi_0^*(-\Delta_0)s^*. \tag{B7}$$

Here again, the local thermal equilibrium condition at the centerline has been applied: $Q_y^*(0) = 0$. When it is combined with the Fourier law and is integrated once with respect to s^*, the following temperature profile can be determined as

$$T^*(s^*) = T^*(0) - \frac{(\gamma - 1)}{2}\mathrm{Pr}\,M^2 T_w^*\Delta_0^2 s^{*2}. \tag{B8}$$

With the first-order Smoluchowski temperature jump at wall surface (2.5),

$$T^*(s^* = 1/2) = T_w^* - \sigma'_{T_C}\mathrm{Kn}T_w^{*-n}\left.\frac{dT^*}{ds^*}\right]_{s^*=1/2}, \tag{B9}$$

the temperature profile can be expressed as

$$T^*(s^*) = T^*(0) - 4\alpha_{T_0}\left[T^*(0) - T_w^*\right] s^{*2} \text{ and } T^*(0) = T_w^*(1 + E_0^2), \tag{B10}$$

where

$$E_0^2 \equiv \frac{(\gamma - 1)}{8\alpha_{T_0}} \Pr M^2 \Delta_0^2, \quad \alpha_{T_0} \equiv \frac{1}{1 + 4\sigma'_{T_C} \mathrm{Kn} T_w^{*-n}}. \tag{B11}$$

Finally, from the equation of state, the density profile can be determined as $\rho^* = T_w^*/T^*$. The temperature can also be expressed in terms of E_0^2 and T_w^*,

$$T^*(s^*) = T_w^* \left[1 + E_0^2 \left(1 - 4\alpha_{T_0} s^{*^2}\right)\right]. \tag{B12}$$

The unknown average temperature T_w^* is then determined by using the second equation in auxiliary relations (3.15); in the case of a Maxwellian molecule ($n = 1$), it is reduced to

$$T_w^* = \left[1 + E_0^2 \left(1 - \frac{\alpha_{T_0}}{3}\right)\right]^{-1}. \tag{B13}$$

Notice that Equation (B13) is coupled with Equations (B5) and (B11), and they comprise a system of nonlinear algebraic equations with two dependent variables Δ_0 and T_w^*. The solution of the system can be determined in terms of Kn and M by a method of iterations. With these solutions, the slip velocity and the temperature jump can be determined from Equations (B3) and (B12), respectively. In addition, through equation $y^* = \int_0^{s^*} T^{*^n}(s^*) ds^*$, the solutions in s^* space can be transformed in the domain of the distance from the wall surface y^*; in the case of a Maxwellian molecule ($n = 1$),

$$\begin{aligned} y^* &= s^* T_w^* \left[1 + E_0^2 \left(1 - \frac{4}{3}\alpha_{T_0} s^{*^2}\right)\right] \text{ or} \\ s^* &= \sqrt{\frac{1 + E_0^2}{\alpha_{T_0} E_0^2}} \cos\left\{\frac{1}{3}\left[\cos^{-1}\left(-\frac{3}{T_w^*}\frac{\sqrt{\alpha_{T_0}} E_0}{(1 + E_0^2)^{3/2}} y^*\right) + 4\pi\right]\right\}. \end{aligned} \tag{B14}$$

Also, the following useful relation can be further derived:

$$\begin{aligned} \frac{du^*}{dy^*} &= \frac{\Delta_0}{T^*} = \frac{\Delta_0}{T_w^*\left[1 + E_0^2\left(1 - 4\alpha_{T_0} s^{*^2}\right)\right]}, \\ \frac{dT^*}{dy^*} &= \frac{T_w^*\left(-8\alpha_{T_0} E_0^2 s^*\right)}{T^*} = -\frac{8\alpha_{T_0} E_0^2 s^*}{1 + E_0^2\left(1 - 4\alpha_{T_0} s^{*^2}\right)}. \end{aligned} \tag{B15}$$

Note that, in contrast with the previous constant coefficient case, *the velocity gradient is not constant and depends not only on the Knudsen number but also on the Mach number and the average temperature T_w^*, meaning that the velocity and temperature profiles, even in the first-order Navier-Stokes-Fourier framework, are tightly interwoven in general*. Analytical solutions of other cases such as $n = 1/2$ (hard sphere), $n = 3/4$, and $n = 4/5$ are summarized in Appendix C.

APPENDIX C: AVERAGE TEMPERATURE IN OTHER GAS MOLECULES

In the case of $n = 1/2$ (hard sphere), $n = 3/4$, and $n = 4/5$, an analytical expression for the average temperature can be developed by using the following integral formula:

$$\int (c_1 - c_2 s^2)^{1/2} ds = \frac{1}{2} s\sqrt{c_1 - c_2 s^2} + \frac{c_1}{2\sqrt{c_2}} \tan^{-1} \frac{\sqrt{c_2} s}{\sqrt{c_1 - c_2 s^2}},$$
$$\int (c_1 - c_2 s^2)^{3/4} ds = \frac{2}{5} s(c_1 - c_2 s^2)^{3/4} + \frac{3}{5} c_1^{3/4} s_2 F_1 \left(\frac{1}{2}, \frac{1}{4}; \frac{3}{2}; \frac{c_2}{c_1} s^2 \right), \tag{C1}$$
$$\int (c_1 - c_2 s^2)^{4/5} ds = \frac{5}{13} s(c_1 - c_2 s^2)^{4/5} + \frac{8}{13} c_1^{4/5} s_2 F_1 \left(\frac{1}{2}, \frac{1}{5}; \frac{3}{2}; \frac{c_2}{c_1} s^2 \right),$$

where the hypergeometric function ${}_2F_1(a, b; c; z)$ is defined as $(-1 < z < 1)$,[46]

$${}_2F_1(a, b; c; z) = 1 + \frac{ab}{1!c} z + \frac{a(a+1)b(b+1)}{2!c(c+1)} z^2 + \cdots. \tag{C2}$$

In the present problem, the constants and variable are defined as

$$c_1 \equiv (1 + E_0^2) T_w^*, \; c_2 \equiv 4\alpha_{T_0} E_0^2 T_w^*, \; z \equiv \frac{c_2}{c_1} s^{*2} = \frac{4\alpha_{T_0} E_0^2}{1 + E_0^2} s^{*2} \tag{C3}$$

and consequently, the condition $-1 < z < 1$ is strictly satisfied. Then, the average temperatures T_w^* can be determined by using the second equation in auxiliary relations (3.15); they are expressed as, in the order of $n = 1/2, 3/4, 4/5$,

$$T_w^* = 4\alpha_{T_0} E_0^2 \left[\sqrt{\alpha_{T_0}} E_0 \sqrt{1 + (1 - \alpha_{T_0}) E_0^2} + (1 + E_0^2) \tan^{-1} \frac{\sqrt{\alpha_{T_0}} E_0}{\sqrt{1 + (1 - \alpha_{T_0}) E_0^2}} \right]^{-2},$$
$$T_w^* = \left\{ \frac{2}{5} \left[1 + (1 - \alpha_{T_0}) E_0^2 \right]^{3/4} + \frac{3}{5} \left(1 + E_0^2 \right)^{3/4} {}_2F_1 \left(\frac{1}{2}, \frac{1}{4}; \frac{3}{2}; \frac{\alpha_{T_0} E_0^2}{1 + E_0^2} \right) \right\}^{-4/3}, \tag{C4}$$
$$T_w^* = \left\{ \frac{5}{13} \left[1 + (1 - \alpha_{T_0}) E_0^2 \right]^{4/5} + \frac{8}{13} \left(1 + E_0^2 \right)^{4/5} {}_2F_1 \left(\frac{1}{2}, \frac{1}{5}; \frac{3}{2}; \frac{\alpha_{T_0} E_0^2}{1 + E_0^2} \right) \right\}^{-5/4}.$$

In addition, the relationships between s^* and y^* can be written as, in the same order,

$$y^* = s^* \frac{\sqrt{T_w^*}}{4} \left[2\sqrt{1 + \left(1 - 4\alpha_{T_0} s^{*2} \right) E_0^2} + \frac{\left(1 + E_0^2 \right)}{s^* \sqrt{\alpha_{T_0}} E_0} \tan^{-1} \frac{2\sqrt{\alpha_{T_0}} E_0 s^*}{\sqrt{1 + \left(1 - 4\alpha_{T_0} s^{*2} \right) E_0^2}} \right],$$
$$y^* = s^* \frac{\left[T_w^* (1 + E_0^2) \right]^{3/4}}{5} \left\{ 2 \left[\frac{1 + \left(1 - 4\alpha_{T_0} s^{*2} \right) E_0^2}{1 + E_0^2} \right]^{3/4} + 3 {}_2F_1 \left(\frac{1}{2}, \frac{1}{4}; \frac{3}{2}; \frac{\alpha_{T_0} E_0^2}{1 + E_0^2} \right) \right\}, \tag{C5}$$
$$y^* = s^* \frac{\left[T_w^* (1 + E_0^2) \right]^{4/5}}{13} \left\{ 5 \left[\frac{1 + \left(1 - 4\alpha_{T_0} s^{*2} \right) E_0^2}{1 + E_0^2} \right]^{4/5} + 8 {}_2F_1 \left(\frac{1}{2}, \frac{1}{5}; \frac{3}{2}; \frac{\alpha_{T_0} E_0^2}{1 + E_0^2} \right) \right\}.$$

Also, the corresponding velocity and temperature gradients for general n can be expressed as

$$\frac{du^*}{dy^*} = \frac{\Delta_0}{T^{*n}} = \frac{\Delta_0}{T_w^{*n} \left[1 + E_0^2 \left(1 - 4\alpha_{T_0} s^{*2} \right) \right]^n},$$
$$\frac{dT^*}{dy^*} = \frac{T_w^* \left(-8\alpha_{T_0} E_0^2 s^* \right)}{T^{*n}} = -\frac{8\alpha_{T_0} E_0^2 s^*}{T_w^{*n-1} \left[1 + E_0^2 \left(1 - 4\alpha_{T_0} s^{*2} \right) \right]^n}. \tag{C6}$$

APPENDIX D: BGK (OR RELAXATION) APPROXIMATION TO THE DISSIPATION TERMS

When an additional approximation is introduced to the dissipation terms in second-order constitutive Equations (2.4) and (3.1), the mathematical analysis can be drastically simplified. It

has been shown in the previous works[34,39] that the factor $q(\kappa)$ plays a minor role in the qualitative behaviors of the constitutive relations in the case of the *velocity shear dominated* flow, as can be observed clearly from its absence in relations (3.5)–(3.7) due to cancellation. Therefore, a first-order linear approximation $q(\kappa) = 1$, which is equivalent to the so-called relaxation time approximation (also known as the BGK approximation in the literature[49]), may be employed for mathematical simplicity. Then, original *implicit* relations (3.11) are simplified into the *explicit* relations as follows:

$$\Pi^*_{xy} = \frac{3}{3+2\left(N_\delta \Pi^*_{xy_0}\right)^2}\Pi^*_{xy_0},\ \Pi^*_{yy} = -\frac{2N_\delta \Pi^*_{xy_0}}{3+2\left(N_\delta \Pi^*_{xy_0}\right)^2}\Pi^*_{xy_0},$$
$$Q^*_y = \frac{3}{3+2\left(N_\delta \Pi^*_{xy_0}\right)^2}Q^*_{y_0},\ Q^*_x = \left(1+\frac{1}{\mathrm{Pr}}\right)\frac{3N_\delta \Pi^*_{xy_0}}{3+2\left(N_\delta \Pi^*_{xy_0}\right)^2}Q^*_{y_0}. \tag{D1}$$

The shear-thinning property, which in turn results in vanishing effective viscosity for increasing Knudsen number, can be easily identified from the first equation of (D1).

[1] R. E. Street, "A study of boundary conditions in slip-flow aerodynamics," in *Rarefied Gas Dynamics*, edited by F. M. Devienne (Pergamon Press, New York, 1960), Vol. 3, p. 276.
[2] R. K. Agarwal, K. Y. Yun, and R. Balakrishnan, "Beyond Navier-Stokes: Burnett equations for flows in the continuum-transition regime," Phys. Fluids **13**(10), 3061 (2001).
[3] J. M. Reese, M. A. Gallis, and D. A. Lockerby, "New directions in fluid dynamics: Non-equilibrium aerodynamic and microsystem flows," Philos. Trans. R. Soc., A **361**, 2967 (2003).
[4] S. Colin, "Rarefaction and compressibility effects on steady and transient gas flows in microchannels," Microfluid. Nanofluid. **1**(3), 268 (2005).
[5] J. M. Reese and Y. Zhang, "Simulating fluid flows in micro and nano devices: The challenge of non-equilibrium behaviour," J. Comput. Theor. Nanosci. **6**(10), 2061 (2009).
[6] L. Zheng, B. C. Shi, and Z. H. Chai, "Lattice Boltzmann method for simulating the temperature jump and velocity slip in microchannels," Commun. Comput. Phys. **2**(6), 1125 (2007).
[7] S. H. Kim and H. Pitsch, "Analytic solution for a higher-order lattice Boltzmann method: Slip velocity and Knudsen layer," Phys. Rev. E **78**(1), 016702 (2008).
[8] N. Dongari, Y. Zhang, and J. M. Reese, "Modeling of Knudsen layer effects in micro/nanoscale gas flows," J. Fluid Eng. **133**(7), 071101 (2011).
[9] W. M. Zhang, G. Meng, and X. Wei, "A review on slip models for gas microflows," Microfluid. Nanofluid. **13**(6), 845 (2012).
[10] W. Marques and G. M. Kremer, "Couette flow from a thirteen field theory with slip and jump boundary conditions," Continuum Mech. Thermodyn. **13**, 207 (2001).
[11] H. Xue, H. Ji, and C. Shu, "Analysis of micro-Couette flow using the Burnett equations," Int. J. Heat Mass Transfer **44**, 4139 (2001).
[12] H. Xue, H. Ji, and C. Shu, "Prediction of flow and heat transfer characteristics in micro-Couette flow," Microscale Thermophys. Eng. **7**, 51 (2003).
[13] T. Thatcher, "Microscale gas flow: A comparison of Grad's 13 moment equations and other continuum approaches," M.S. thesis, University of Victoria, 2005.
[14] M. Torrilhon, "Two-dimensional bulk microflow simulations based on regularized Grad's 13-moment equations," Multiscale Model. Simul. **5**(3), 695 (2006).
[15] L. O'Hare, D. A. Lockerby, J. M. Reese, and D. R. Emerson, "Near-wall effects in rarefied gas micro-flows: Some modern hydrodynamic approaches," Int. J. Heat Fluid Flow **28**(1), 37 (2007).
[16] K. Xu and H. Liu, "Multiscale gas-kinetic simulation for continuum and near continuum flows," Phys. Rev. E **75**, 016306 (2007).
[17] S. Mizzi, "Extended macroscopic models for rarefied gas dynamics in micro-sized domains," Ph.D. thesis, University of Strathclyde, 2008.
[18] C. R. Lilley and J. E. Sader, "Velocity gradient singularity and structure of the velocity profile in the Knudsen layer according to the Boltzmann equation," Phys. Rev. E **76**, 026315 (2007).
[19] D. A. Lockerby, J. M. Reese, D. R. Emerson, and R. W. Barber, "Velocity boundary condition at solid walls in rarefied gas calculations," Phys. Rev. E **70**, 017303 (2004).
[20] D. A. Lockerby, J. M. Reese, and M. A. Gallis, "The usefulness of higher-order constitutive relations for describing the Knudsen layer," Phys. Fluids **17**, 100606 (2005).
[21] D. A. Lockerby, J. M. Reese, and M. A. Gallis, "Capturing the Knudsen layer in continuum fluid models of nonequilibrium gas flows," AIAA J. **43**, 1391 (2005).
[22] D. A. Lockerby and J. M. Reese, "On the modelling of isothermal gas flows at the microscale," J. Fluid Mech. **604**, 235 (2008).
[23] H. Grad, "On the kinetic theory of rarefied gases," Commun. Pure Appl. Math. **2**, 331 (1949).
[24] H. Grad, "The profile of a steady plane shock wave," Commun. Pure Appl. Math. **5**, 257 (1952).
[25] R. E. Khayat and B. C. Eu, "Nonlinear transport processes and fluid dynamics: Cylindrical Couette flow of Lennard-Jones fluids," Phys. Rev. A **38**(5), 2492 (1988).

[26] B. C. Eu, *Kinetic Theory and Irreversible Thermodynamics* (Wiley, New York, 1992).
[27] B. C. Eu, *Generalized Thermodynamics: The Thermodynamics of Irreversible Processes and Generalized Hydrodynamics* (Kluwer Academic Publishers, Dordrecht, 2002).
[28] D. Burnett, "The distribution of molecular velocities and the mean motion in a non-uniform gas," Proc. London. Math. Soc. **40**, 382 (1935).
[29] S. Chapman and T. G. Cowling, *The Mathematical Theory of Nonuniform Gases*, 3rd ed. (Cambridge University Press, Cambridge, 1970).
[30] K. Xu, "Super-Burnett solutions for Poiseuille flow," Phys. Fluids **15**(7), 2077 (2003).
[31] K. Xu and Z. Li, "Microchannel flow in the slip regime: Gas-kinetic BGK-Burnett solutions," J. Fluid Mech. **513**, 87 (2004).
[32] R. S. Myong, "Thermodynamically consistent hydrodynamic computational models for high-Knudsen-number gas flows," Phys. Fluids **11**(9), 2788 (1999).
[33] R. S. Myong, "A generalized hydrodynamic computational model for rarefied and microscale diatomic gas flows," J. Comput. Phys. **195**, 655 (2004).
[34] R. S. Myong, "A full analytical solution for the force-driven compressible Poiseuille gas flow based on a nonlinear coupled constitutive relation," Phys. Fluids **23**, 012002 (2011).
[35] R. S. Myong, "Impact of computational physics on multi-scale CFD and related numerical algorithms," Comput. Fluids **45**, 64 (2011).
[36] N. T. P. Le, H. Xiao, and R. S. Myong, "A triangular discontinuous Galerkin method for non-Newtonian implicit constitutive models of rarefied and microscale gases," J. Comput. Phys. **273**, 160 (2014).
[37] H. Xiao and R. S. Myong, "Computational simulations of microscale shock-vortex interaction using a mixed discontinuous Galerkin method," Comput. Fluids **105**, 179 (2014).
[38] L. Boltzmann, "Further studies on the thermal equilibrium of gas molecules," Sitzungsber. Akad. Wiss. **66**, 275 (1872).
[39] R. S. Myong, "On the high Mach number shock structure singularity caused by overreach of Maxwellian molecules," Phys. Fluids **26**(5), 056102 (2014).
[40] E. Meeron, "Series expansion of distribution functions in multicomponent fluid systems," J. Chem. Phys. **27**, 1238 (1957).
[41] R. Kubo, "Generalized cumulant expansion method," J. Phys. Soc. Jpn. **17**, 1100 (1962).
[42] T. Ree and H. Eyring, "Theory of non-Newtonian flow. I. Solid plastic system," J. Appl. Phys. **26**, 793 (1955).
[43] K. L. Johnson and J. L. Tevaarwerk, "Shear behaviour of elastohydrodynamic oil films," Proc. R. Soc. A **356**, 215 (1977).
[44] R. S. Myong, "Gaseous slip model based on the Langmuir adsorption isotherm," Phys. Fluids **16**(1), 104 (2004).
[45] J. C. Maxwell, "On stresses in rarefied gases arising from inequalities of temperature," Philos. Trans. R. Soc. London **170**, 231 (1879).
[46] M. von Smoluchowski, "Uber den temperaturesprung bei warmeleitung in gasen," Sitzungsber. Akad. Wiss. **107**, 304 (1898).
[47] M. Abramowitz and C. A. Stegun, *Handbook of Mathematical Functions with Formulas, Graphs, and Mathematical Tables* (Dover Publication, New York, 1972).
[48] P. L. Bhatnagar, E. P. Gross, and M. Krook, "A model for collision processes in gases. I," Phys. Rev. **94**, 511 (1954).
[49] G. A. Bird, *Molecular Gas Dynamics and the Direct Simulation of Gas Flows* (Clarendon Press, Oxford, 1994).
[50] A. Karchani and R. S. Myong, "Convergence analysis of the direct simulation Monte Carlo based on the physical laws of conservation," Comput. Fluids **115**, 98 (2015).
[51] O. Ejtehadi, E. Roohi, and J. A. Esfahani, "Detailed investigation of hydrodynamics and thermal behavior of nano/micro shear driven flow using DSMC," Sci. Iran., B **20**, 1228 (2013).
[52] M. Tij and A. Santos, "Combined heat and momentum transport in a dilute gas," Phys. Fluids **7**(11), 2858 (1995).
[53] J. M. Montanero, A. Santos, and V. Garzó, "Monte Carlo simulation of nonlinear Couette flow in a dilute gas," Phys. Fluids **12**(11), 3060 (2000).